https://dx.doi.org/10.1016/j.ensm.2021.09.034

Research Progress of MXene-based Catalysts for Electrochemical Water-splitting and Metal-air Batteries

Jingyuan Qiao [a], Lingqiao Kong [a], Shaokang Xu [a], Kaixian Lin [a], Wei He [a, *], Meng Ni [b], Qiushi Ruan [a], Peigen Zhang [a, *], Ying Liu [c], Wei Zhang [a], Long Pan [a], ZhengMing Sun [a, *]

[a] *Jiangsu Key Laboratory of Advanced Metallic Materials, School of Materials Science and Engineering, Southeast University, Nanjing 211189, China*

[b] *Building Energy Research Group, Department of Building and Real Estate, The Hong Kong Polytechnic University Hung Hom, Kowloon, Hong Kong 999077, China*

[c] *Jiangsu JITRI Advanced Polymer Materials Research Institute Co., Ltd., Nanjing 211800, China*

* Corresponding authors.

E-mail addresses:

zmsun@seu.edu.cn (ZhengMing Sun)

weih@seu.edu.cn (Wei He)

zhpeigen@seu.edu.cn (Peigen Zhang)

Declaration of interest

The authors declare that they have no known competing financial interests or personal relationships that could have appeared to influence the work reported in this paper.

Acknowledgements

This study was supported by Natural Science Foundation of Jiangsu Province (grant no. BK20200406), National Natural Science Foundation of China (grant no. 51731004), the grants (Project no.: PolyU 152064/18E) from Research Grant Council, University Grants Committee, Hong Kong SAR, and Project of Strategic Importance Program of The Hong Kong Polytechnic University (Project ID: P0035168).

Research Progress of MXene-based Catalysts for Electrochemical Water-splitting and Metal-air Batteries

Abstract

MXenes, a rising family of two-dimensional (2D) materials, are characterized by a unique combination of high electrical conductivities, hydrophilicity, and adjustable surface properties, which exhibit great potential in overall water splitting and metal-air batteries as electrocatalysts. In this review, the preparation methods, and some relevant properties of MXenes are summarized, and their application in electrocatalysis are systematically reviewed from theoretical calculations to experimental investigations, including hydrogen evolution reaction (HER), oxygen evolution reaction (OER), oxygen reduction reaction (ORR), and bifunctional activity. The strategies for improving their electrocatalytic performance and electrocatalytic mechanisms are discussed, and the challenges and prospects relative to the applications of MXenes in electrocatalysis are also presented.

Keywords: MXenes, electrocatalysis, water-splitting, metal-air batteries

1 Introduction

Increasing energy and environmental issues have promoted the exploration of green, renewable energies, such as solar and wind energies [1, 2]. However, the outputs of those renewable energies heavily depend on the weather and climate conditions [3, 4]. To obtain steady electricity, efficient and low-cost energy conversion, or storage technologies such as water splitting and metal-air batteries are necessary, and such technologies strongly rely on the availability of efficient electrocatalysts [5, 6]. Generally, noble metals, such as platinum and ruthenium, exhibit excellent catalytic activity [7, 8]. However, low reserves and high costs have severely restricted the large-scale application. Therefore, the development of efficient no-noble metal catalysts is of importance for electrocatalysis.

Among the no-noble metal catalysts, like transition-metal oxides [9, 10], hydroxide [11, 12], sulfide [13, 14], phosphides [15] and so on [16, 17], two-dimensional (2D) materials have attracted much attention because of their unique electronic and structural characteristics, high specific surface area, and structural adjustability [18]. Graphite-like carbon nitride (g-C_3N_4) [17], 2D transition metal dichalcogenides (TMDs) [19], black phosphorus (BP) [20] and layered double hydroxides (LDHs) [12, 21] have been applied in the field of catalysis for energy conversion, including hydrogen evolution reaction (HER), oxygen evolution/reduction reaction (OER/ORR), carbon dioxide reduction reaction (CO_2RR), and nitrogen reduction reaction (NRR) [22-26].

However, those developed catalysts have some obvious drawbacks, including poor electrical conductivity, slow charge transfer, and instability of active sites [26, 27].

MXenes are a new family of 2D transition metal carbides, nitrides, and carbonitrides, which are regarded as the next promising candidate for electrocatalysis [28]. Compared with other 2D materials, MXenes have received increasing attention due to their electrical conductivity (10000 S cm^{-1}), compositional diversity, thin and tunable structure, easily adjustable surface, and hydrophilic nature [29, 30]. MXenes are derived from their MAX precursors, having a general formula of $M_{n+1}X_nT_x$ (n = 1, 2 or 3), where M represents transition metals (e.g., Ti, V, Cr, Mo, Nb, and so on), X stands for C or N, T denotes the functional groups (e.g., -O, -OH and -F) [30, 31]. A large number of stable MXenes have been predicted theoretically, and more than 30 types have already been synthesized from corresponding MAX [31-34]. The tunability of the composition of MXenes is beneficial for electronic structure modulation, and the unique 2D layered structure provides a large specific surface area and maximally exposes the active sites [35, 36]. In addition, the excellent corrosion resistance and hydrophilicity expand the range of application compared to carbon-based supports [37, 38]. The functional groups greatly facilitate the assembly of MXene nanosheets, and strongly interact with other materials, which can effectively avoid the aggregation of nanomaterials and optimize the electronic structure of MXene-based hybrids [39-42]. Based on the above, MXenes show great promise as electrocatalysts and support for energy conversion.

In 2016, Mo_2CT_x and $Ti_3C_2T_x$ were reported for the first time as HER and OER catalysts respectively [43, 44]. Since then, the number of MXene-related papers in the water splitting and metal-air batteries field has been increasing year by year, showing an explosive trend (**Figure 1** (a)). Meanwhile, excellent electrocatalytic performances have been found. For example, the $Mo_2TiC_2T_x$ anchored single Pt atoms ($Mo_2TiC_2T_x$-Pt_{SA}) as HER catalyst required an overpotential of only 30 mV to reach a current density of 10 mA cm^{-2} [45], the Fe-N-C/MXene superlattice-like heterostructure showed a comparable half-wave potential (0.84 V) to Pt/C benchmark (0.90 V) [46], and the $Ni_{1-x}Fe_xPS_3$ nano-mosaic-decorated MXene hybrids revealed low overpotential (282 mV) for OER in 1 M KOH [47].

To date, a host of MXenes related reviews have been published with emphasis on MXenes preparation, interfacial structure design, and potential applications [35, 48-53]. As shown in **Figure 1** (b), this review introduces the synthesis of MXenes and focuses on the progress of MXenes application in electrocatalysis, including HER, OER, ORR, and bifunctional activity (HER/OER and OER/ORR). The strategies to improve the electrocatalytic performance of MXenes and hybrids are comprehensively discussed, including surface functional groups control, defect engineering, heteroatom doping, active materials loading, and hybrid nanostructure design. Moreover, challenges and prospects of MXene in electrocatalytic applications are addressed.

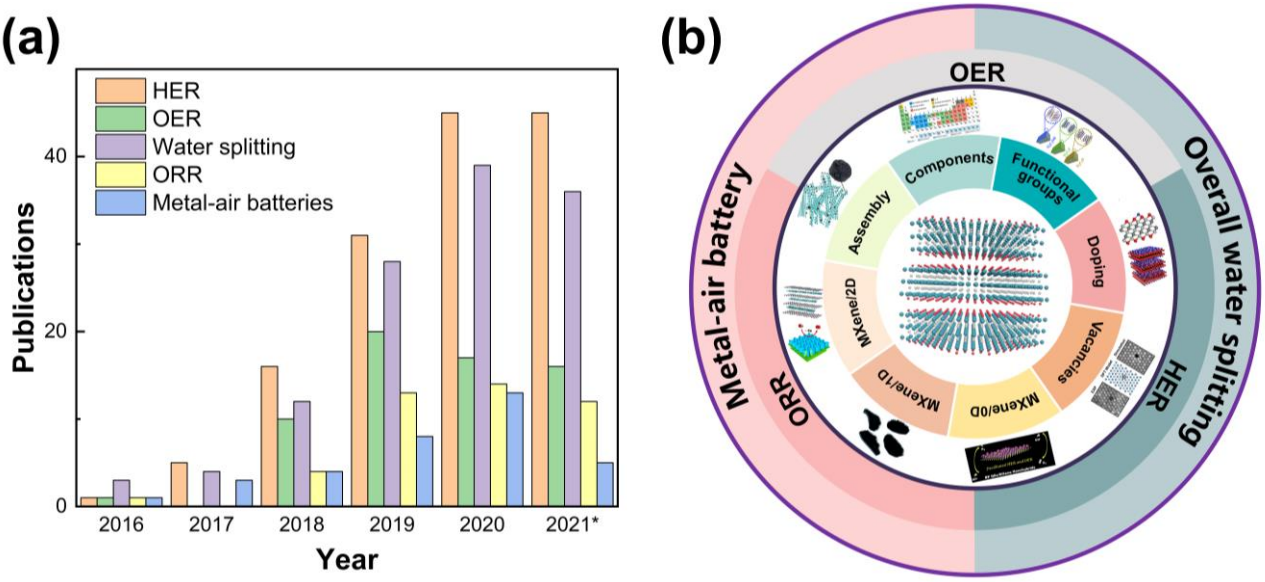

Figure 1. (a) The histogram of the MXene related publications over time for HER, OER, ORR, overall water splitting, and metal-air batteries on Web of Science. 2021* means that the statistics are as of August 2021. (b) Illustration of the potential applications of MXenes and hybrids electrocatalysts. (Components image. Reproduced with permission [54]. Copyright 2019, American Chemical Society. Functional groups image. Reproduced with permission [55]. Copyright 2020, Elsevier Ltd. Doping image. Reproduced with permission [56, 57]. Copyright 2018, American Chemical Society, Copyright 2020, WILEY-VCH. Vacancies image. Reproduced with permission [58]. Copyright 2016, American Chemical Society. MXene/0D image. Reproduced with permission [59]. Copyright 2018, Royal Society of Chemistry. MXene/1D image. Reproduced with permission [15]. Copyright 2019, Royal Society of Chemistry. MXene/2D image. Reproduced with permission [46, 60]. Copyright 2020, American Chemical Society, Copyright 2017, Elsevier Ltd. Assembly image. Reproduced with permission [61]. Copyright 2019, American Chemical Society.)

2 Synthesis and properties of MXenes

2.1 Synthesis

MXenes are usually produced by selectively etching the A layers in the corresponding MAX precursors [32, 62, 63]. The MAX, short for $M_{n+1}AX_n$ (n = 1, 2, or 3), represents a large family of carbides/nitrides or carbonitrides, consisting of alternatively stacked MX and A layers. In their formula, M and X are the same as in MXenes, and A represents the III/IV A group elements (e.g., Al, Ga, Si, and Ge) [30]. Within the MAX phase, M-A metallic bonds are weaker and more active than M-X bonds [29]. Accordingly, 2D MXenes can be obtained by preferentially destroying the M-A bonds and retaining the M-X structure [30, 64].

In 2011, Naguib *et al.* synthesized the first MXene (Ti_3C_2) by etching Ti_3AlC_2 in HF solution (**Figure 2** (a)) [29]. Hereafter, Ti_2CT_x, V_2CT_x, Mo_2CT_x, Nb_2CT_x, $Zr_3C_2T_x$, $Mo_2TiC_2T_x$, and several other MXenes were successfully prepared using the same method [32, 49, 63]. Until now, HF etching is still the most classic and common method for MXenes preparation. However, due to the strong corrosiveness and high toxicity of HF, environmentally friendly and safe methods are urgently needed. In 2014, the mixed solution of LiF and HCl was developed as the etchant to synthesize $Ti_3C_2T_x$ [65]. Then, the same product was obtained by using the mixed solutions of other fluorides and acids as an etchant, such as H_2SO_4, NaF, and even NH_4HF_2 [66, 67]. Besides, molten fluoride salts were also an option for the etchant, and Ti_4N_3 was successfully produced by using it (**Figure 2** (b)) [68]. To further avoid fluoride, alkali treatment, hydrothermal assistance, and even electrochemical etching were developed to obtain fluorine-free MXene [69-73]. Taking electrochemical etching as an example, within the etching process, dilute hydrochloric acid acted as the etchant, and the MAX phases were successfully etched under gentle heating, resulting in a unique flower-like architecture of MXene [74]. And the newly emerging Lewis acidic molten salt etching is also worthy of attention. Ti_3AlC_2 and Ti_2AlC were etched by $ZnCl_2$ under Ar atmosphere to form Cl-terminated Ti_3C_2 and Ti_2C, respectively (**Figure 2** (c)) [75]. And this strategy can also be extended to a broader range. For example, Ta_2C can be synthesized by etching Ta_2AlC using AgCl [76]. Moreover, to control the defects and microstructures, bottom-up methods such as chemical vapor deposition (CVD) were also employed to synthesize high-quality MXenes, which exhibited excellent application prospects (**Figure 2** (d)) [77-79]. Different methods introduce different functional and morphologies, which obviously influence their characteristics, properties, and performance [80].

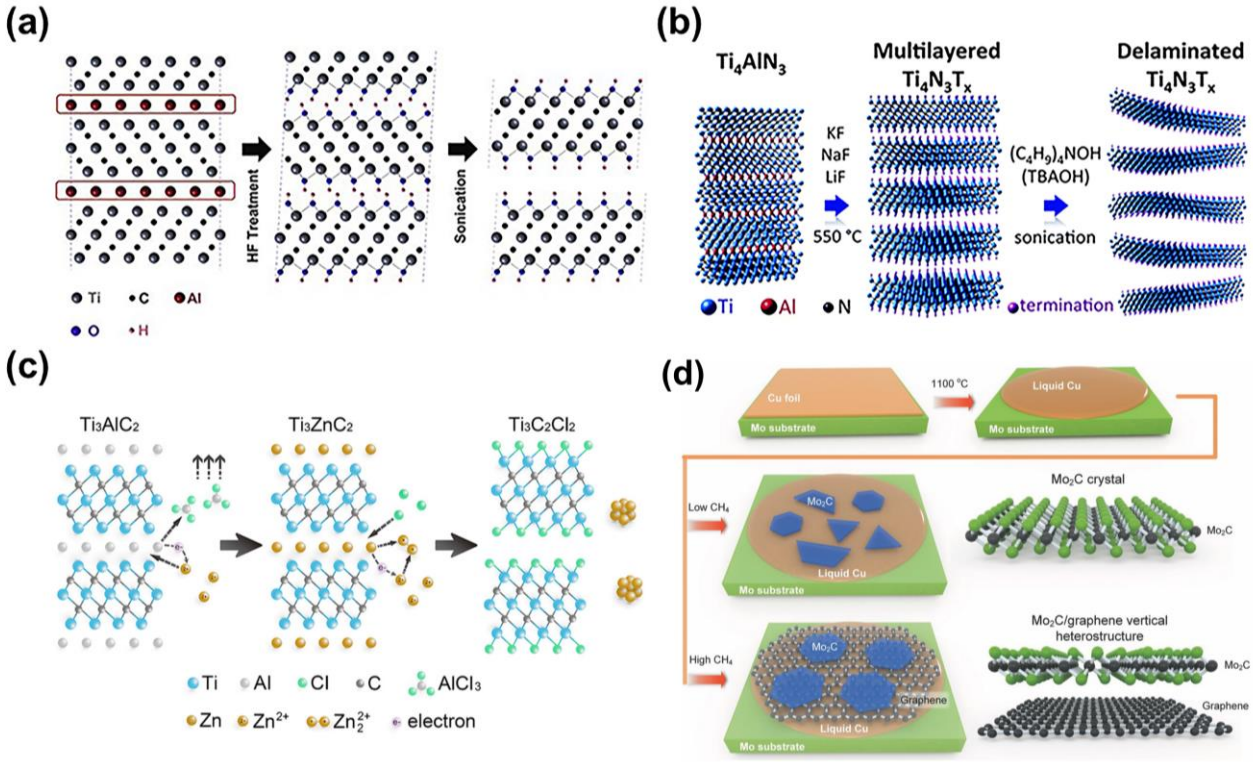

Figure 2. (a) Schematic of the exfoliation process for Ti_3AlC_2 by HF treatment. Reproduced with permission [29]. Copyright 2011, WILEY-VCH. (b) Schematic illustration of the synthesis of $Ti_4N_3T_x$ by molten salt treatment. Reproduced with permission [68]. Copyright 2016, Royal Society of Chemistry. (c) Schematic of Lewis acid ($ZnCl_2$) etching Ti_3AlC_2 to prepare Ti_3C_2. Reproduced with permission [75]. Copyright 2019 American Chemical Society. (d) The growth of Mo_2C crystals by CVD. Reproduced with permission [79]. Copyright 2017, WILEY-VCH.

2.2 Structure and properties

MXenes inherit the M-X structure from their MAX phase precursors, and the M layers have a hexagonal structure similar to graphene, while the X atoms occupy the octahedral interstitials constructed by the M atoms [81]. As seen in **Figure 3**, MXenes currently have three structures: M_2XT_x, $M_3X_2T_x$, and $M_4X_3T_x$, where M layer can be sole-element or multi-elements [31, 82]. And two types of element distribution are found in the multiple element case: solid solutions and ordered distribution. For solid solutions, the multiple elements are randomly distributed within the M layers, while the ordered one appears as two ways: out-of-plane order and in-plane order [83-85]. In addition, X can also be mixed, such as C and N in Ti_3CN [86]. The large number of MAX phase members and their solid solutions provide a huge composition space for MXenes, implying tunability on their properties and performance. The weak van der Waals interaction between the multi-layer MXenes can be easily overcame through ultrasonic treatment and intercalation, yielding few-layer or even single-layer MXenes, accompanied by the increased specific surface area, which

is beneficial to the application in catalysis and energy storage [87, 88]. Many cations, including Na^+, K^+, NH_4^+, $Al^{3+}$and Mg^{2+}, have proven to be intercalators to enlarge the interlayer distance (**Figure 4** (a)) [89]. And the (0 0 2) distance of $Ti_3C_2T_x$ could increase 5.1 Å after placing in KOH (**Figure 4** (b)). Besides, dimethyl sulfoxide (DMSO), dimethylformamide (DMF), and tetrabutylammonium hydroxide (TBAOH) also perform well to intercalate and enhance delaminating MXenes [90, 91].

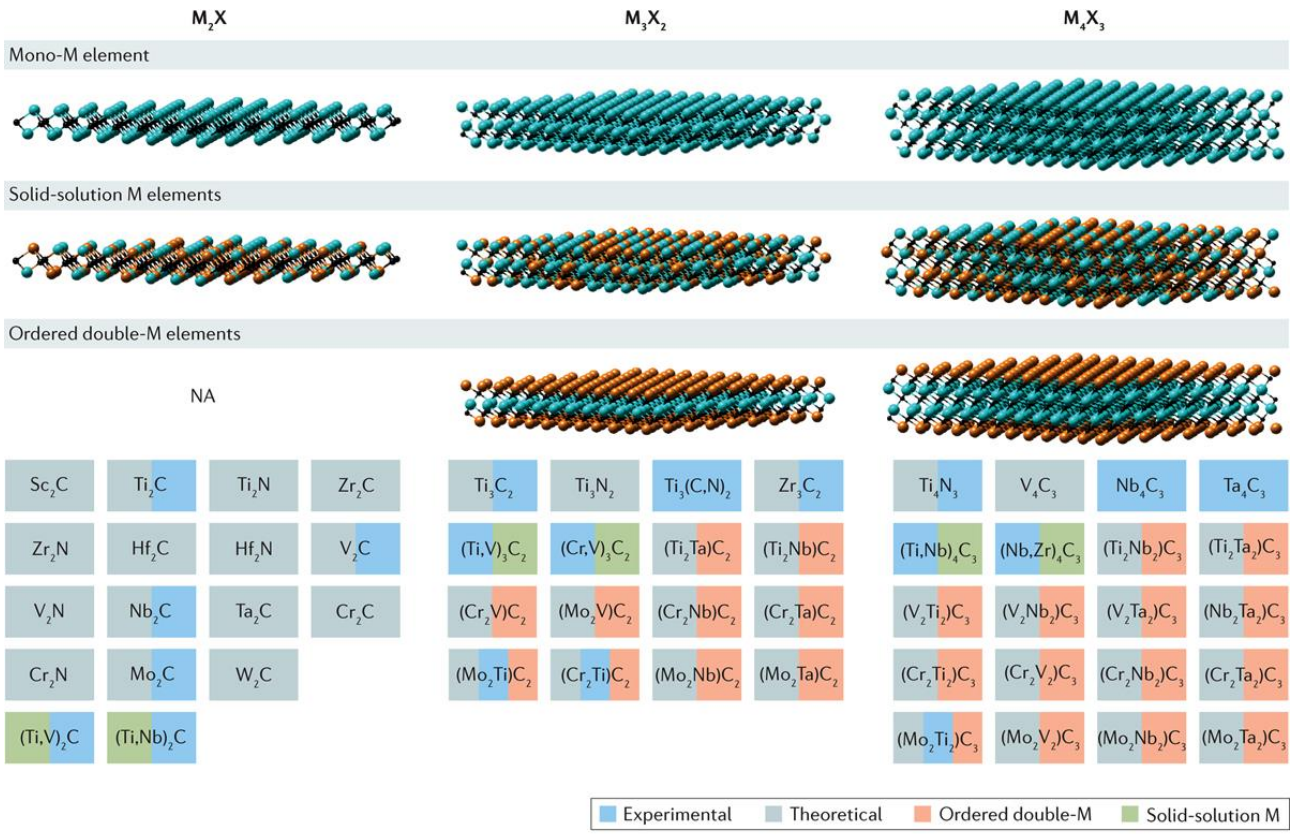

Figure 3. Different types of MXenes. Reproduced with permission [31]. Copyright 2017, Springer Nature.

The functional groups left on MXenes during the synthesis processes strongly affect their chemical properties [92, 93]. The hydrophilic polar groups such as -OH and -O, facilitate MXenes interacting with solution. In addition, the electrical properties of MXenes strongly correlate with their functional groups [94]. For example, all the ideally bare MXenes are metallic, which become semiconductors after being functionalized like Ti_2CO_2, Ti_3C_2F, Zr_2CO_2, and so on [28, 94]. Further, the surface de-functionalization can be observed with in-situ electron energy loss spectroscopy (EELS) and has been confirmed to improve the conductivity of the synthesized MXenes [95]. And the -O/-OH ratio also influenced the HER performance of $W_{1.33}CT_x$ [96]. With the in-depth understanding of the effect of functional groups on MXenes, the adjustment of functional groups has attracted much attention. Recently, Kamysbayev *et al.* adjusted the functional groups on Ti_3C_2 by molten salt etching [97]. O-terminated, NH-terminated, S-terminated, Cl-terminated, Se-

terminated, Br-terminated, Te-terminated, and even bare MXenes (may be H-terminated) were successfully prepared (**Figure 4** (c)). Control of functional groups on MXenes can optimize their properties, and the effect on their electrocatalytic performance will be discussed in the subsequent sections. Beside the functional groups, MXenes inevitably contain vacancy defects even synthesized by a mild method [58, 98]. From the STEM images (**Figure 4** (d)), the single Ti atom vacancy and two adjacent Ti vacancies in the same sublayers could be clearly observed in $Ti_3C_2T_x$. And the formation energies of Ti vacancy clusters and single Ti vacancies were calculated in **Figure 4** (e). The two formation energies were proportional to the number of vacancies, and the small formation energy difference suggested that large vacancy clusters formed feasibly. The defect engineering in MXenes is a common strategy to improve their electrocatalysis performances. For example, defects affect the electronic properties of surrounding sites and can trap single-atom as effective catalysts [45, 96, 99-101].

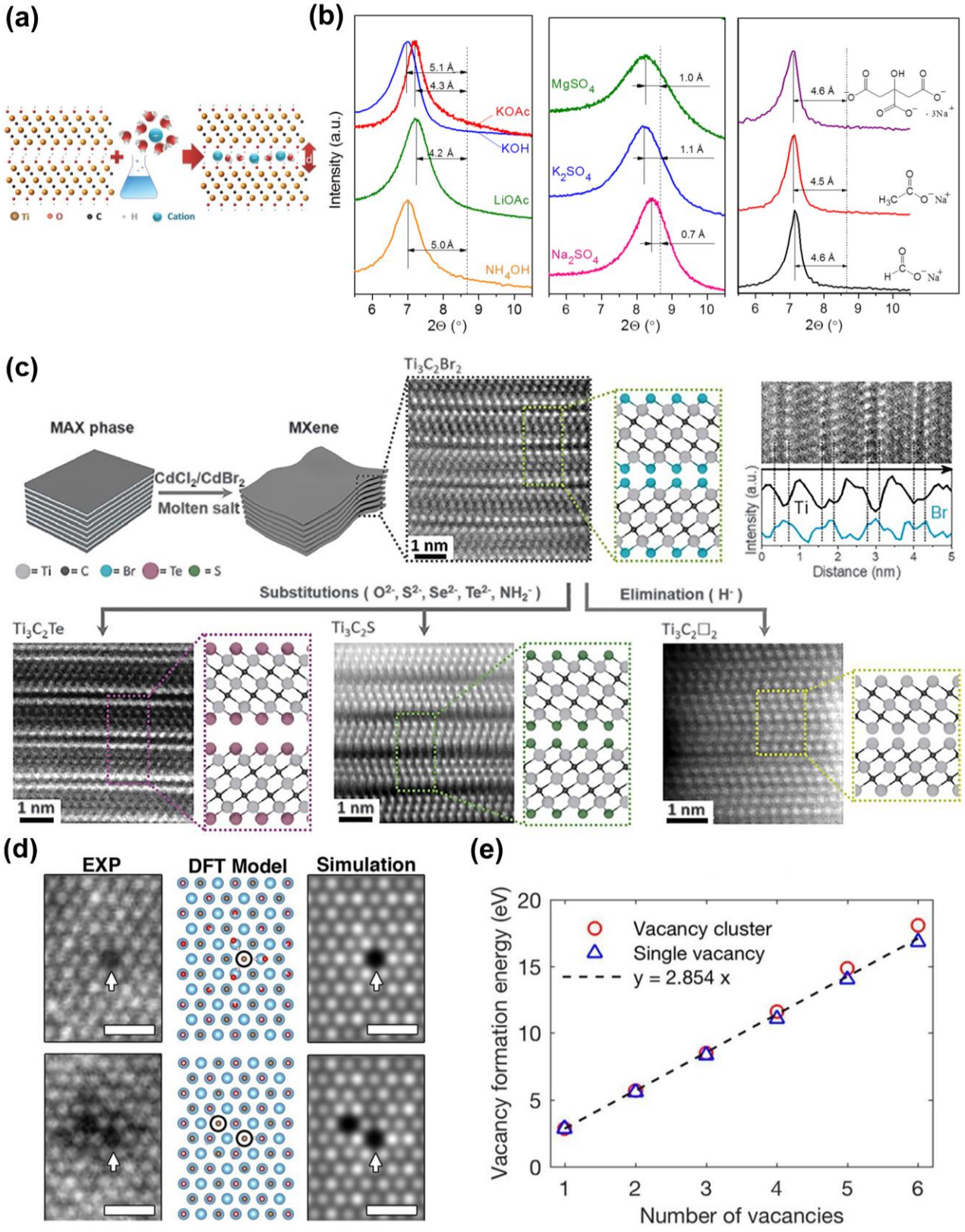

Figure 4. (a) Schematic illustration of cations intercalation between $Ti_3C_2T_x$ layers. (b) XRD of $Ti_3C_2T_x$ after placing in various salts. Reproduced with permission [89]. Copyright 2013, American Association for the Advancement of Science. (c) Surface reactions of MXenes in molten inorganic salts. Reproduced with permission [97]. Copyright 2020, American Association for the

Advancement of Science. (d) Comparison between experimental HAADF-STEM images, DFT model, and simulated HAADF-STEM images of atomic-scale defects in $Ti_3C_2T_x$. Scale bars are 0.5 nm. (e) The formation energy of Ti vacancy clusters as a function of the number of Ti vacancies. Reproduced with permission [58]. Copyright 2016, American Chemical Society.

3 MXene-based catalysts for electrochemical water-splitting and metal-air batteries

3.1 Electrochemical water-splitting

Water electrolysis produces hydrogen (H_2) and oxygen (O_2) on the cathode and anode accompanied with hydrogen evolution reaction (HER) and the oxygen evolution reaction (OER), respectively. Hydrogen, a clean and environmentally friendly energy source, is expected to be an ideal energy carrier for renewable energy storage to address the global energy crisis and environmental problems [102, 103]. As mentioned above, MXenes exhibit unique advantages compared with other electrochemical catalysts [28, 43]. Meanwhile, the abundant functional groups on MXenes also make it possible to couple with other active materials. Therefore, higher activity can be achieved with the interface regulation and the synergy between the different components of the hybrids. In this section, MXene-based catalysts for electrochemical water-splitting are introduced in the aspects of HER, OER, and bifunctional reaction. And the electrochemical performances are summarized in **Table 2, Table 3,** and

Table *4*, respectively.

3.1.1 Catalysts for HER

Usually, HER occurs via the Volmer-Heyrovsky route or the Volmer-Tafel route [104]. During HER, H atoms first adsorb on the surface of the electrode through the Volmer reaction, and then H_2 molecules are released from the interface through the Heyrovsky reaction or Tafel reaction (**Table 1**). In HER, the bond of H_{ads} on the electrode plays a key role [105], and it should not be too weak (limiting Volmer reaction) or too strong (limiting Heyrovsky or Tafel reaction). Therefore, HER catalysts can be evaluated by the Gibbs free energy (ΔG_H) for hydrogen adsorption.

Due to the good hydrophilicity, chemical resistance, and reducibility, MXenes are regarded as potential catalysts for HER [85, 106]. Compared with the common 2D HER catalysts such as MoS_2, MXenes demonstrates basal-plane activity and high electrical conductivity, which leads to more effective catalyst utilization [107, 108]. Therefore, the functional groups on the basal-plane affect the HER activity of MXenes significantly, which is proved by theoretical calculations. Li *et al.* found that the abundant F-termination on Ti_2C reduced the positive ΔG_H value, promoting the adsorption kinetics of protons. And the F-termination reduced the charge transfer resistance [109]. Pan *et al.* investigated the H and O functional group effect on MXenes (Mo_2X and W_2X, X = C and

N) based on density-functional-theory (DFT) calculations [110]. It was claimed that the bare and H-terminated W_2C monolayers showed near-zero overpotential with high H-coverage, and the oxidization of Mo_2X could enhance the HER activity. More research results showed that -O/-OH groups were more favorable to HER. Ling *et al.* claimed that Ti_2CO_2 and W_2CO_2 had comparable ΔG_H ($|\Delta G_H|$~0.12eV) with Pt (111) surface ($|\Delta G_H|$~0.09eV) [111]. By establishing a volcanic map between the total HER rate and Gibbs free energy of hydrogen adsorption/N_e (the number of electrons obtained by surface O atoms), a simple descriptor N_e was used to evaluate the HER performance of O-terminated MXenes. And $TiVCO_2$ was identified as a highly active catalyst by the simple descriptor. Moreover, the descriptor can be extended to other systems [112, 113]. Once the optimal electron numbers are determined, the HER catalysts with high activity can be effectively screened or designed. And Gao *et al.* showed that MXenes with -O/-OH groups were stable and metallic by DFT calculation, which was favorable for charge transfer [28]. The surface oxygen atoms at the top and bottom of MXene were the active sites of HER, and H* showed a suitable interaction strength with the MXenes (**Figure 5** (a)), which was also confirmed experimentally [92]. Furthermore, S/P partial replacement of the O functional groups on Ti_2CO_2 can significantly improve its HER performance [114].

Due to the large variety of MXenes, machine learning (ML) has been used to efficiently screen MXene-based catalysts [115-117]. Zheng *et al.* combined DFT calculation with ML to perform high-throughput screening of bare and S-terminated MXenes [118]. Os_2B and S-terminated $Sc_{n+1}N_n$ (n = 1, 2, 3) showed excellent activity to HER, and ΔG_H was close to zero under wide hydrogen coverage among 299 different kinds of MXenes. Besides the modulation of functional groups, a family of ordered double transition-metal MXenes has also been screened and selected by ML [106, 119]. And 110 kinds of candidates were selected from 2520 MXenes [120]. The combination of high-throughput calculations and precise predictions of ML provides a shortcut for the exploration of MXene-based catalysts.

Table 1. HER mechanism in alkaline and acidic media.

	Alkaline media	**Acidic media**	**Tafel slop ($mV\ dec^{-1}$)**
Volmer	$* + H_2O + e^- \rightarrow *H + OH^-$	$* + H^+ + e^- \rightarrow *H$	~120
Heyrovsky	$* + H_2O + e^- + *H \rightarrow H_2 + OH^- + *$	$* + H^+ + e^- + *H \rightarrow H_2 + *$	~40
Tafel	$2*H \rightarrow 2* + H_2$	$2*H \rightarrow 2* + H_2$	~30
Overall	$* + 2H_2O + 2e^- \rightarrow H_2 + 2OH^-$	$* + 2H^+ + 2e^- \rightarrow H_2$	

The catalytic activity of MXenes could be adjusted by regulating the transition-metal atom layers or vacancies. The change of hydrogen adsorption energy could reach 0.5 eV by changing the number of metal layers of MXenes, suggested by a theoretical calculation (**Figure 5** (b, c)) [121]. And Cheng *et al.* found that the appropriate introduction of carbon vacancies adjusted HER activity [122]. As shown in **Figure 5** (d), the ΔG_H of V_C-Cr_2CO_2 decreased with increasing carbon vacancy concentration (8.33%~25%), indicated that carbon vacancies particularly with low concentration could weaken the binding strength between H atoms and Cr_2CO_2, enhancing HER activity. The appropriate vacancies concentration may be beneficial [45], but too many vacancies can negatively affect the HER performance. The $Mo_{1.33}CT_x$ with ordered Mo vacancies exhibited lower HER activity (422 mV) than Mo_2CT_x, which delivered a 239 mV overpotential at 10 mA cm^{-2} (**Figure 5** (e)) [123]. And as represented in **Figure 5** (f), the change of coordination structure by the loss of the favorable site for the HER process induced the decline of HER performance.

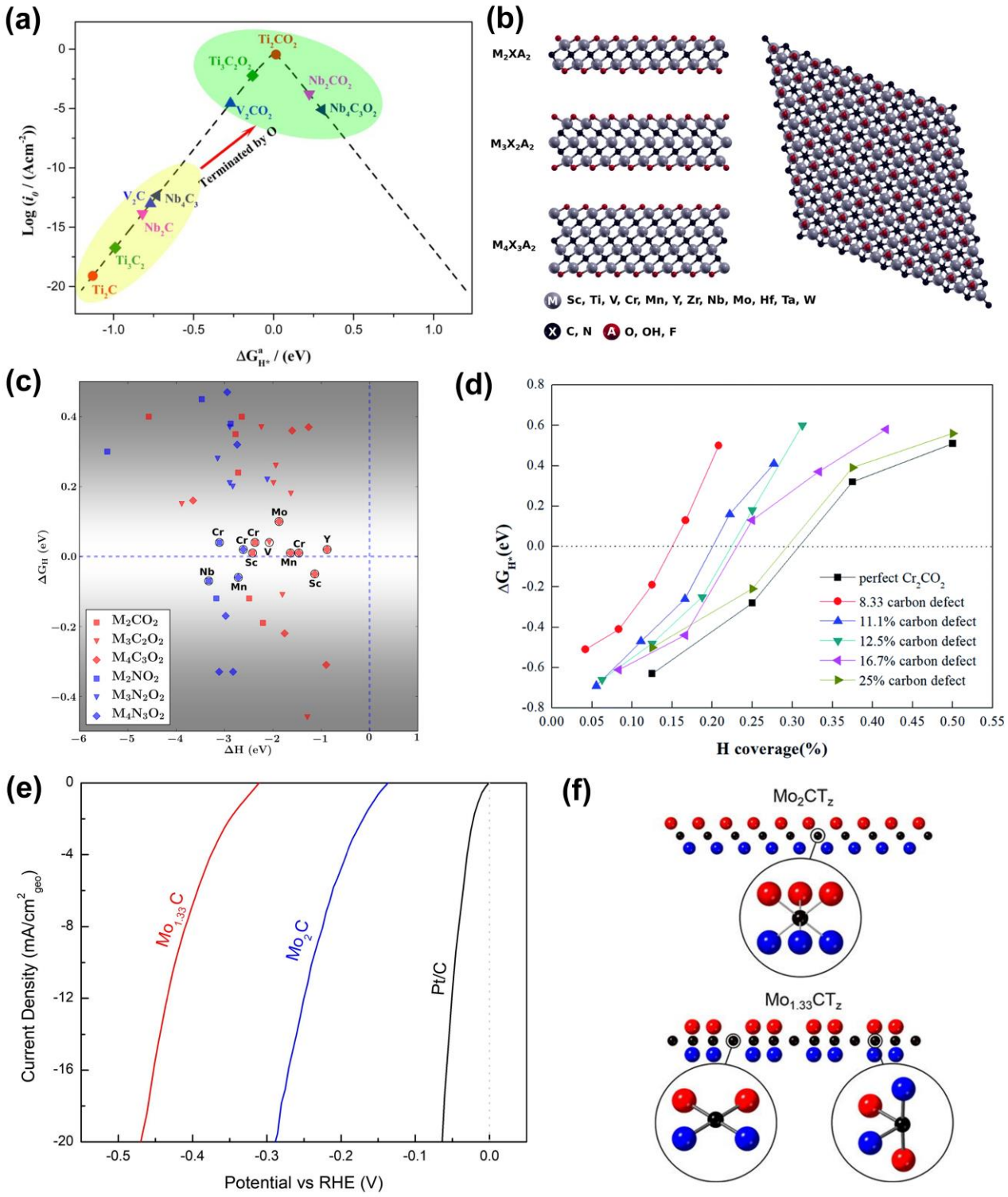

Figure 5. (a) Volcano curve of exchange current (i_0) and the average Gibbs free energy of hydrogen adsorption ($\Delta G^{a}_{H^*}$). Reproduced with permission [28]. Copyright 2016, American Chemical Society. (b) Ball-and-stick model of MXenes with different layer thickness. (c) ΔH versus ΔG_H plot for MXenes that have $|\Delta G_H| \leq 0.5$ eV. The circled data points denote the compounds that have $|\Delta G_H| \leq 0.1$ eV. Reproduced with permission [121]. Copyright 2017, American Chemical Society. (d) The ΔG_{H^*} at different concentrations of carbon vacancies of V_C-Cr_2CO_2 as a function of H coverage. Reproduced with permission [122]. Copyright 2018, Royal Society of Chemistry. (e) Polarization

curves for $Mo_{1.33}CT_z$ and Mo_2CT_z. (f) Side view (along b-direction) of Mo_2C and $Mo_{1.33}C$. Reproduced with permission [123]. Copyright 2019, Elsevier.

Besides the functional groups and vacancies, the heteroatoms doping is one of the most feasible strategies to enhance the HER activity of 2D materials [13, 124]. Doping MXenes with heteroatoms can adjust its electronic properties, surface chemistry, and element composition. Although O-terminated MXenes have been shown good HER activity, the high hydrogen bonding strength also limits its performance, especially for V_2CO_2 and $Ti_3C_2O_2$. Therefore, doping with the low electronegativity non-metallic atoms may be an appropriate option. Le *et al.* synthesized the N-doped $Ti_3C_2T_x$ by the conventional ammonia heat-treatment method [125]. The introduction of nitrogen modified the electronic configuration by decreasing the electron densities of oxygen sites, because of the enhanced interaction between Ti and N. The appropriate nitrogen content increased its conductivity and catalytic activity. And its catalytic performance was presented in **Figure 6** (a), the onset potential of N-$Ti_3C_2T_x$@600 was -30 mV, and its overpotential at 10 mA cm^{-2} was only 198 mV. The DFT calculation also confirmed that ΔG_H could be adjusted to the ideal value (0 eV) by optimizing the nitrogen content. In addition, P-doped MXenes also showed favorable performance [56]. Phosphating treatment introduced P and O at the same time on the interlayer surfaces of each Mo-C-Mo monolayer in Mo_2CT_x and expanded the interlayer spacing. P and O co-doped Mo_2CT_x had improved conductivity, and thus exhibited better performance than Mo_2CT_x. The P-doped Mo_2CT_x exhibited a low overpotential (only 186 mV at 10 mA cm^{-2}, much better than that of Mo_2CT_x). Similarly, V_2CT_x after P doping showed better HER activity [126]. The doping of P can lead the electron transfer to the anti-bonding orbital of V-H/O-H to motivate the activity of V_2CT_x. And P-C bands could act as the active sites, which moderately reduced the bonding strength of H_{ads} and promoted the desorption. Thus, the P-V_2CT_x exhibited the low overpotential (163 mV at 10 mA cm^{-2}) and Tafel slope (74 mV dec^{-1}) in 0.5 M H_2SO_4. Like doping with the low electronegativity non-metallic atoms, doping with the metallic electron donors such as some transition metals can also enhance the HER activity of MXenes. The interaction between H and O was alleviated by introducing some other transition-metals atoms on the V_2CO_2 surface [127]. The transfer of electrons from the transition-metal atoms to the surface O could weaken the bonding between O and H, and therefore, the ΔG_H could be optimized to ~0 eV by choosing the suitable transition-metals atoms and coverage [128]. After modification, the ΔG_H of Os-Ta_2CO_2, Ir-Sc_2CO_2, Ag-Nb_2NO_2, Re-Nb_2NO_2, and W-Nb_2NO_2 were close to 0 eV. And the redistribution of surface electrons caused by the transition-metal atoms made the HER mechanism preferred Volmer-Tafel to Volmer-Heyrovsky. Furthermore, replacing the Mo atoms in the Mo_2CT_x lattice by Co atoms resulted in Mo_2CT_x:Co [129], and the introduction of Co atoms regulated the bond energy of O and

H around the Co sites. At least 9 neighboring surface oxygen groups could be activated by one substitution Co atom, and therefore, the Mo_2CT_x: Co performed better than Mo_2CT_x. Recently, single Pt atoms were successfully introduced into $Mo_2TiC_2T_x$ (**Figure 6** (b)) [45]. Mo vacancies on the $Mo_2TiC_2T_x$ basal surface were introduced by electrochemical exfoliation, while Pt atoms were anchored into the vacancies to form the stable single atoms catalysts ($Mo_2TiC_2T_x$-Pt_{SA}). As shown in **Figure 6** (c), when the current densities were 10, 20, and 100 mA cm^{-2}, the overpotentials of $Mo_2TiC_2T_x$-Pt_{SA} were 30, 77, and 104 mV, respectively, better than that of commercial Pt/C. Due to the emergence of new Pt sites, $Mo_2TiC_2T_x$-Pt_{SA} showed a fast kinetic process with a Tafel slope. And DFT calculation also showed that the confined, single Pt atoms in the lattice redistributed the electronic structure, effectively improved the *d*-electron domination near the Fermi level, and thus enhanced the HER catalytic activity.

The combination of MXenes and other active materials is also worthy of attention. Generally, MXenes can be used as good conductive supports to facilitate charge transfer. It can also be used as a co-catalyst to optimize the adsorption of H to achieve better HER activity through the synergy between different components and the adjustment of the electronic structure. Pt_3Ti intermetallic compound (IMC) nanoparticles (NPs) were synthesized in situ anchored on $Ti_3C_2T_x$ [130]. The in-situ X-ray absorption spectroscopy and the fitting EXAFS spectra revealed the coordination numbers (CNs) of Pt/$Ti_3C_2T_x$-550 (6.6 Pt-Pt bonds and 3.4 Pt-Ti bonds) which also confirmed the formation of Pt_3Ti at 550 °C. And the Pt/$Ti_3C_2T_x$-550 showed the best catalytic performance. The Ti-C structure was well preserved in Pt/$Ti_3C_2T_x$-550, and the Pt_3Ti particles on Pt/$Ti_3C_2T_x$-550 tended to form cubic octahedral morphology, mainly exposing the (111) and (100) crystal planes. Consistent with the DFT calculation results, (111) and (100) surfaces of Pt_3Ti nanoparticles exhibited comparable H binding ability to (111) of Pt. Pt/$Ti_3C_2T_x$-550 delivered a similar kinetics process to Pt/C. And as shown in (**Figure 6** (d)), the specific activity of Pt/$Ti_3C_2T_x$-550 was 13 times that of Pt/C under the same overpotential (70 mV). The overpotential was only 32.7 mV (at 10 mA cm^{-2}) with 32.3 mV dec^{-1} Tafel slope. Similarly, MXene-supported $Co_{0.31}Mo_{1.69}C$ nanoparticles [131], PtNi nanowires [132], and NiCo alloy [133] also demonstrated excellent HER activity, since MXene effectively avoided agglomeration and stacking of low-dimensional materials [134]. On this basis, enhanced HER activity in alkaline media (**Figure 6** (e)) was achieved by combining Co-doped MoS_2 and Mo_2CT_x through heterostructure engineering [107]. Mo_2CT_x served as both the active material and conductive substrate, and the surface functional groups tightened the bonds between MXene and MoS_2, improving structural stability. Meanwhile, the synergistic effects between Co-MoS_2 and Mo_2CT_x led to low charge-transfer resistance. As represented in **Figure 6** (f), the overpotential of Co-MoS_2/Mo_2CT_x was only 112 mV at 10 mA cm^{-2} and the performance remained stable in the alkaline medium up to 18 hours. In addition to heterogeneous structural

engineering, proper 3D structural design can also expand the active sites of nanohybrids. Wu *et al.* vertically arranged MoS_2 nanosheets on Ti_3C_2 MXene to form MoS_2/Ti_3C_2-MXene@C (**Figure 6** (g)) [135]. As a conductive substrate, MXene improved the electrical conductivity while avoiding the agglomeration of MoS_2. The carbon layers can effectively prevent the oxidation of MXene, and the chemical bonds between functional groups and MoS_2 ensured structural stability and rapid charge transfer. And the vertically aligned MoS_2 nanosheets provided more active sites and short paths for mass diffusion and charge transfer. As expressed in **Figure 6** (h), the nanohybrids performed the platinum-like onset potential (20 mV) and overpotential (135 mV at 10 mA cm^{-2}) in 0.5 M H_2SO_4 due to the synergy effect among MXene, MoS_2, and carbon layers. In conclusion, an ideal structure with enhanced HER activity should well retain the MXenes structure to achieve good conductivity and stability, ensure a large surface area and expose more HER active sites.

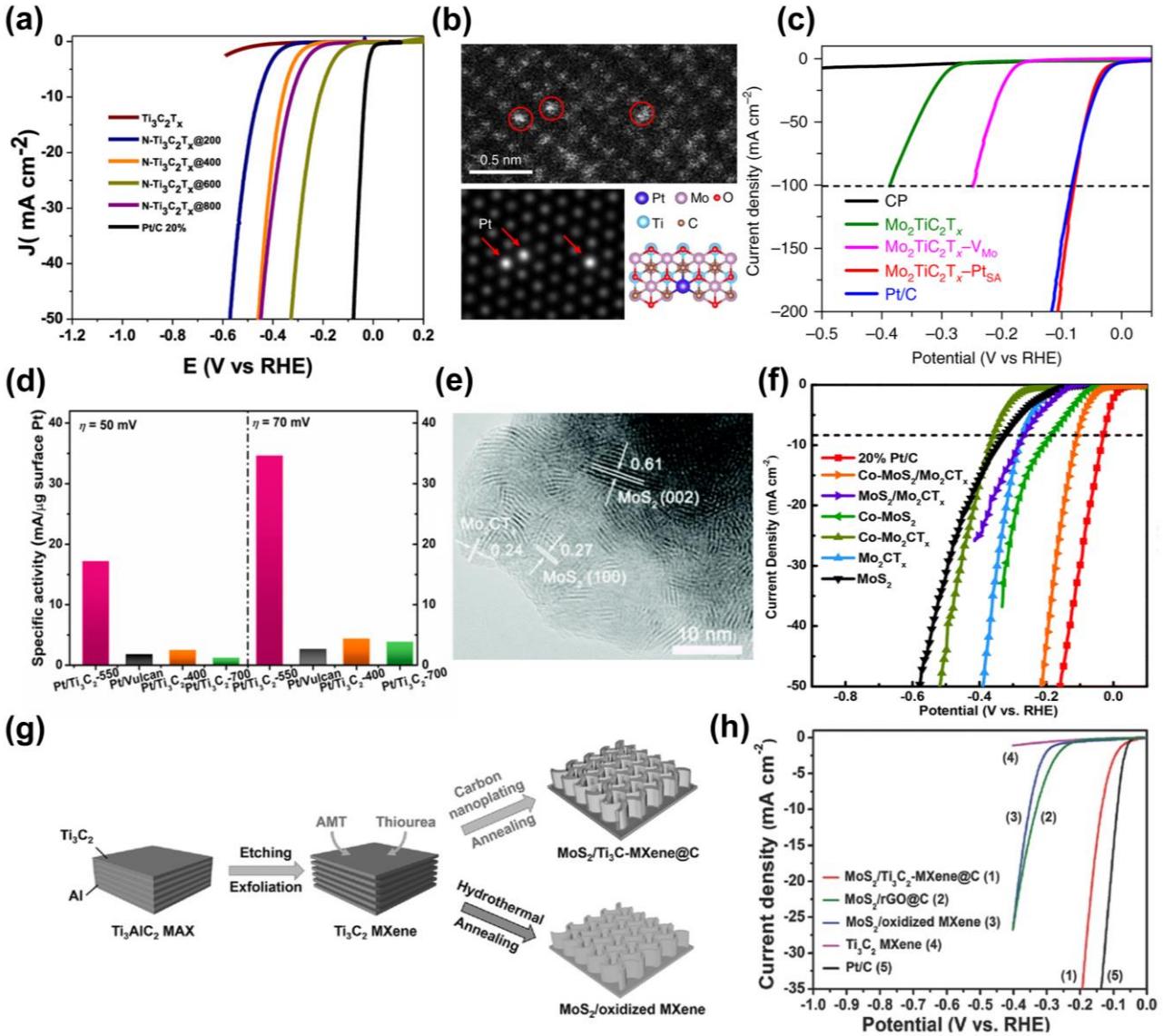

Figure 6. (a) HER polarization curves of $Ti_3C_2T_x$, Pt/C (20%), and N-doped $Ti_3C_2T_x$ catalysts. Reproduced with permission [125]. Copyright 2019, American Chemical Society. (b) HAADF-

STEM image, simulated image, and the structure illustration of $Mo_2TiC_2T_x$-Pt_{SA}. (c) HER polarization curves of carbon paper (CP), $Mo_2TiC_2T_x$-V_{Mo}, $Mo_2TiC_2T_x$-Pt_{SA} and Pt/C (40%) in 0.5 M H_2SO_4 (counter electrode: graphite rod). Reproduced with permission [45]. Copyright 2018, Springer Nature. (d) The specific activity of the Pt/Vulcan and Pt/$Ti_3C_2T_x$ catalysts. Reproduced with permission [130]. Copyright 2019, American Chemical Society. (e) HRTEM image of Co-MoS_2/Mo_2CT_x. (f) The polarization curves of catalysts in 1 M KOH. Reproduced with permission [107]. Copyright 2019, Royal Society of Chemistry. (g) The formation process of MoS_2/Ti_3C_2-MXene@C nanohybrids. (h) Polarization curves of MoS_2/Ti_3C_2-MXene@C, and other catalysts in 0.5 M H_2SO_4. Reproduced with permission [135]. Copyright 2017, WILEY-VCH.

Table 2. Summary of the HER performance metrics of MXene-based hybrids.

Electrocatalyst	Electrolyte	$\eta_{j=10\ mA\ cm^{-2}}$ (mV)	Tafel slope (mV dec^{-1})	Ref.
E-$Ti_3C_2O_x$	0.5 M H_2SO_4	190	60.7	[92]
$Mo_{1.33}CT_x$	0.1 M $HClO_4$	422		[123]
N-$Ti_3C_2T_x$@600	0.5 M H_2SO_4	198	92	[125]
P-Mo_2CT_x	0.5 M H_2SO_4	186		[56]
Mo_2CT_x: Co	1.0 N H_2SO_4	180		[129]
$Mo_2TiC_2T_x$-Pt_{SA}	0.5 M H_2SO_4	30	30	[45]
Pt/$Ti_3C_2T_x$-550	0.1 M $HClO_4$	32.7	32.3	[130]
$Co_{0.31}Mo_{1.69}C$/MXene/NC	1.0 M KOH 0.1 M PBS 0.5 M H_2SO_4	75 126 81	43 46 24	[131]
$Pt_{3.21}Ni$@Ti_3C_2	0.5 M H_2SO_4 1.0 M KOH	18.55 55.6 ($\eta_{j=5}$)	13.3 39.5	[132]
$Ni_{0.9}Co_{0.1}$@$Ti_{2.5}Nb_{0.5}C_2T_x$	1.0 M KOH	43.4	116	[133]
Co-MoS_2/Mo_2CT_x	1.0 M KOH	112	82	[107]
MoS_2/Ti_3C_2-MXene@C	0.5 M H_2SO_4	135	45	[135]
$NiSe_2$/$Ti_3C_2T_x$	0.5 M H_2SO_4	200	37.7	[136]
NiS_2/V_2CT_x	1.0 M KOH	179	85	[14]

NiFe-LDH/$Ti_3C_2T_x$	1.0 M KOH	132	70	[137]
P-V_2CT_x	0.5 M H_2SO_4	220	74	[126]
Ru_{SA}-N-S-$Ti_3C_2T_x$	0.5 M H_2SO_4	76	90	[138]
Ru-SA/$Ti_3C_2T_x$	0.1 M $HClO_4$	70	27.7	[57]
Ru_{SA}-N-$Ti_3C_2T_x$	1.0 M KOH 0.5 M H_2SO_4 1.0 M PBS	27 23 81	29 35	[139]
VS_2-V_2CT_x	1.0 M KOH 0.5 M H_2SO_4	164 ($\eta_{j=20}$) 138	47.6 37.9	[140]
MoS_2/Ti_3C_2 nanoroll	0.5 M H_2SO_4	152	70	[141]
MoS_2/Mo_2CT_x	1.0 M KOH	176 ($\eta_{j=20}$)	207	[142]
CoS_2@MXene	0.1 M KOH	175	97	[143]
CoP/Ti_3C_2 MXene	1.0 M KOH 0.5 M H_2SO_4	102 71	68.7 57.6	[144]
TBA-$Ti_3C_2T_x$-Pt	0.5 M H_2SO_4	55	65	[134]
Pt NP-$Ti_3C_2T_x$	0.5 M H_2SO_4	226	59.5	[145]
MoS_2-Ti_3C_2 MXene	0.5 M H_2SO_4	98	45	[146]
$MoSe_2$/MXene-O	0.5 M H_2SO_4	171	61	[147]
Pd/Nb_2C-HF	0.5 M H_2SO_4	34	34	[148]
$Ti_3C_2T_x$@Pt/SWCNTs	0.5 M H_2SO_4	62	78	[149]
MD-Ti_3C_2/MoS_x	0.5 M H_2SO_4	196 ($\eta_{j=50}$)	41	[150]

3.1.2 Catalysts for OER

The kinetic process of OER, another half-reaction of water splitting, is more sluggish than that of HER. Generally, OER is a four-electrons transfer process which can be described as $4OH^- \rightarrow 2H_2O + O_2 + 4e^-$ (in alkaline) or $2H_2O \rightarrow 4H^+ + O_2 + 4e^-$ (in acidic) [151]. Taking the OER in an alkaline medium as an example, it can be specifically divided into the formation and deprotonation of hydroxides ($OH^- + * \rightarrow *OH + e^-$, $OH^- + *OH \rightarrow *O + H_2O + e^-$) as well as the formation and

deprotonation of peroxides ($OH^- + *O \rightarrow *OOH + e^-$, $OH^- + *OOH \rightarrow * + O_2 + H_2O + e^-$). Besides, it is also possible to obtain O_2 through the reaction of the adjacent *O [152]. Whether it is through the direct combination of *O to produce O_2 or the decomposition of the intermediate (*OOH), the bonding (*-O) within the intermediates (*OH, *O, *OOH) is critical to the overall electrocatalytic capability [153]. For sites with weak *-O, the formation of peroxides may limit the rate of the reaction. And for sites with strong *-O, the deprotonation of the peroxides may limit the progress of the reaction. Therefore, the proper bonding strength between the active sites and O is the key to an efficient OER [154]. Moreover, the rapid mass transfer and high-speed charge transfer can also promote the reaction. The excellent conductivity and chemical resistance of MXenes can ensure the rapid electron transfer and stability during OER. Generally, MXenes have low inherent OER activity, which may be due to the few active sites. And nitrogen doping is a facile strategy to improve the electrochemical performance of MXenes [155, 156]. By etching the corresponding X-site MAX solid solution, N atoms can be easily introduced into MXenes (e.g., $Ti_3C_{1.8}N_{0.2}$ and $Ti_3C_{1.6}N_{0.4}$) [157]. The N atoms in the $Ti_3C_{1.6}N_{0.4}$ provided abundant active sites and effectively improved the electrical conductivity and wettability. N-Q (bond with three C neighbors) and N-6 (in the six-membered heterocyclic ring) greatly improved the electrocatalytic activity. The electron-donor properties of N-6 and the defects introduced by N atoms insertion adjusted the electronic and surface properties to optimize the adsorption energy in the reaction, leading to the enhanced catalytic performance. And the better hydrophilicity of $Ti_3C_{1.6}N_{0.4}$ improved the accessibility to the electrolyte and increased available sites (**Figure 7** (a)). The low onset potential (η_{onset} = 245.8 mV) and Tafel slope (216.4 mV dec^{-1}) proved that the improvement of in-situ nitrogen doping for the OER performance of MXene, and also pointed out the direction for the subsequent optimization of MXenes catalytic performance.

MXenes can also serve as a good carrier to reach high-efficiency OER activity by coupling with other active materials. The ultra-low work function and negatively-charged surface ensure the strong interface interaction among different components, thereby effectively avoiding the aggregation of active materials and improving the stability [42, 158, 159]. Due to the strong interaction and metal conductivity, MXenes are usually employed as support for LDHs and transition metal oxides, which are poorly conductive and easily agglomerate, but highly active [160, 161]. And this combination effectively avoids the limitations of the hydrophobicity of traditional carbon-based carriers to aqueous catalysis. Moreover, the strong coupling between the different components can even optimize the electronic structure of MXene-based hybrids to show better OER activity [137]. And MXene nanosheets facilitate the design of hierarchical structures, which not only provide a large specific surface area to expose more active sites but also provide smooth pathways for the reactants diffusion to improve OER performance [39, 162].

As mentioned above, constructing a hybrid MXene catalyst with different dimensional catalysts is a common strategy to improve the OER performance. The Co_3O_4 particles were combined with MXene through electrostatic self-assembly and solvothermal, effectively avoiding particle aggregation and exposing more active sites [159]. At the same time, the existence of MXene greatly shortened the mass transfer and charge transfer paths. The synergy between the 0D Co_3O_4 and 2D Ti_3C_2 greatly improved the OER activity, and the overpotential at 10 mA cm^{-2} is only 300 mV with a low Tafel slope of 118 mV dec^{-1}. 2D metal-organic framework (MOF) nanosheets are also considered to be potential catalysts for OER, but poor electrical conductivity limits their applications. Combining 2D MOFs with MXene is also expected to achieve better electrocatalytic performance. Cobalt 1,4-benzenedicarboxylate (CoBDC) and $Ti_3C_2T_x$ nanosheets were compounded to obtain $Ti_3C_2T_x$-CoBDC by interdiffusion reaction [163]. The well-defined interface and synergistic effect between $Ti_3C_2T_x$ and CoBDC effectively improved the kinetic process. And the high conductivity of $Ti_3C_2T_x$ changed the limiting step of OER on CoBDC from the charge-transfer process to the reaction-limited process, with a low Tafel slope (48.2 mV dec^{-1}). As shown in **Figure 7** (b), $Ti_3C_2T_x$-CoBDC achieved the current density of 10 mA cm^{-2} at 1.64 V in alkaline. Similarly, the same strategy to further improve layered double hydroxide (LDH) catalytic activity was investigated [164]. The electrodeposited CoNi-LDH loaded on the nickel foam coated with MXene also achieved good OER performance [161]. MXene modulated the electronic structure of CoNi-LDH, and the strong electronic interaction affected the d-band centers of Ni and Co, which optimized the adsorption strength of the reaction intermediate and improved the OER performance.

The structure of catalysts can greatly affect the mass transfer, and a 3D MXene based structure with suitable pore channel distribution and tortuosity accelerates the mass transfer to improve the OER performance. As shown in **Figure 7** (c), g-C_3N_4 and MXene were stacked to form flexible films with a self-supporting structure (TCCN) [44]. And the pores in TCCN also provided a smooth pathway for reactants transferring (e.g., -OH) and reaction products releasing (e.g., O_2). NEXAFS and XPS indicated that Ti-N_x reduced the electron density of Ti atoms, forming Ti-N_x active sites which facilitated the adsorption of OH^- in alkaline media. The OER that occurred on TCCN was controlled by the 4-electron pathway with high faraday efficiency (95.5%). As shown in **Figure 7** (d), the TCCN film electrode showed a comparable working potential (1.65 V) to IrO_2/C (1.70 V) at 10 mA cm^{-2}. The current attenuation was lower (4.3%) than that of IrO_2/C (29.7%), and no phase or morphology changed after 10 hours testing. The vertically arranged layered cobalt borates on the MXene (Co-B_i/$Ti_3C_2T_x$) exposed more active sites and significantly improved mass diffusion and charge transfer [165]. $Ti_3C_2T_x$ greatly suppressed the aggregation of Co-B_i and the chemical bonding between MXene and Co-B_i nanosheets promoted the spontaneous charge transfer of Co-B_i/$Ti_3C_2T_x$. Therefore, the adsorption of the intermediate was promoted to achieve a rapid

oxidation-reduction process and exhibited excellent OER activity (Tafel slope was only 53 mV dec^{-1} and the overpotential was 250 mV at 10 mA cm^{-2}). This strategy can also be extended to other 2D materials such as LDH [166, 167]. The in-situ vertical growth of CoFe-LDH on Ti_3C_2 MXene led to the "house of cards" structure [166]. The strong combination between LDH and MXene promoted electron transfer and improved structural stability. As expressed in **Figure 7** (e), the MXene hybrid exhibited a superb electrocatalytic performance with an overpotential of 319 mV at a current density of 10 mA cm^{-2} and a Tafel slope of 50 mV dec^{-1}. Similarly, Yu *et al.* obtained FeNi-LDH/Ti_3C_2-MXene by ionic hetero-assembly of FeNi-LDH and Ti_3C_2-MXene (**Figure 7** (f)) [60]. After hybridization with Ti_3C_2, the d-band center of Ni/Fe atoms in FeNi-LDH/Ti_3C_2-MXene was shifted to higher energy, leading to the enhancement of the O bonding strength. Thus, the charge transfer in the whole OER was accelerated. And the FeNi-LDH/Ti_3C_2-MXene showed a lower overpotential of 298 mV than RuO_2 (358 mV) at 10 mA cm^{-2} (**Figure 7** (g)).

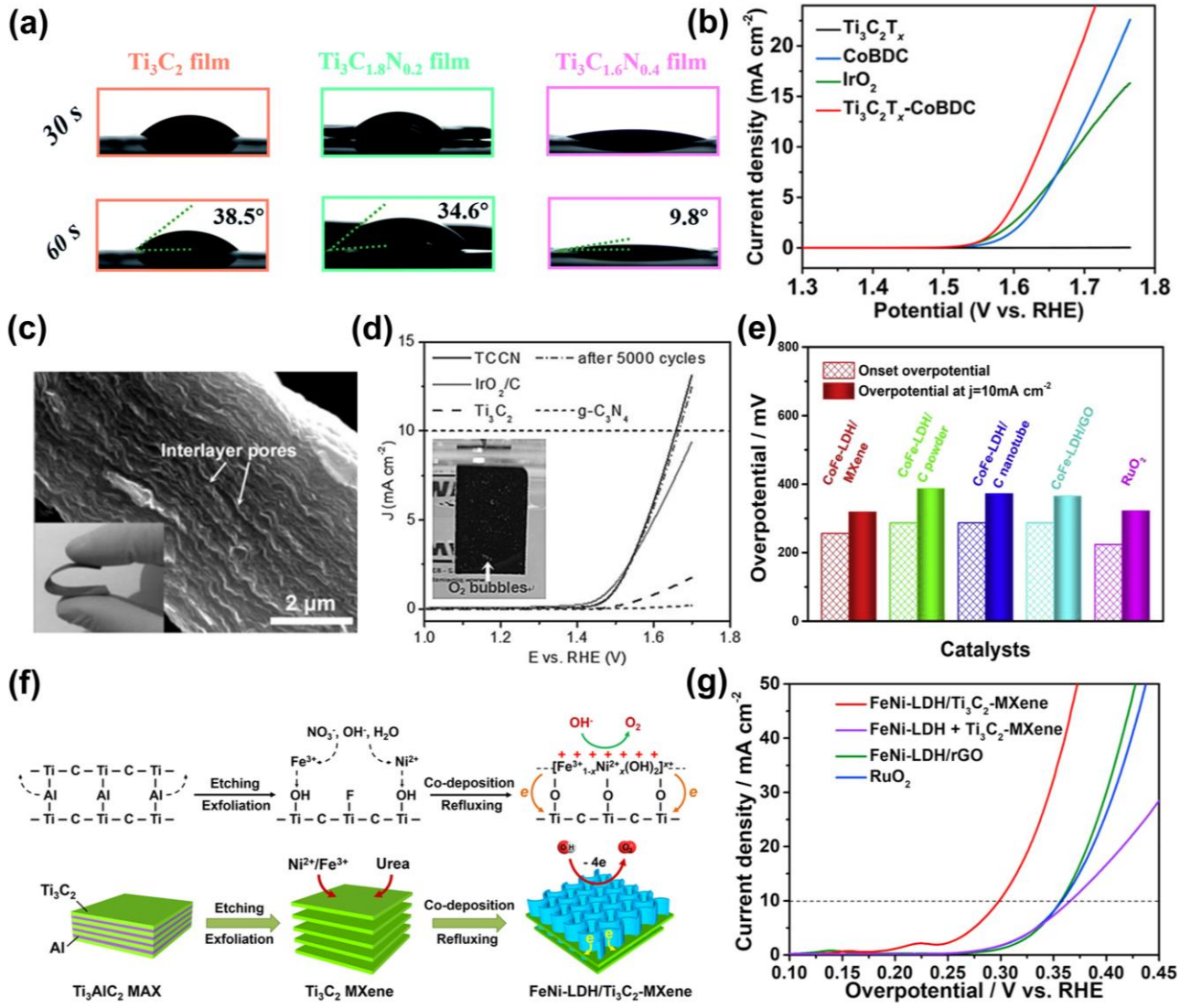

Figure 7. (a) The contact angles of 1 M KOH electrolyte for Ti_3C_2 film, $Ti_3C_{1.8}N_{0.2}$ film, and $Ti_3C_{1.6}N_{0.4}$ film. Reproduced with permission [157]. Copyright 2020, Royal Society of Chemistry. (b) OER polarization curves of $Ti_3C_2T_x$, CoBDC, IrO_2, and $Ti_3C_2T_x$-CoBDC hybrid in 0.1 M KOH

(N_2-saturated) with a scan rate of 1 mV s^{-1}. Reproduced with permission [163]. Copyright 2017, American Chemical Society. (c) SEM and optical (inset) images of TCCN film. (d) Polarization curves, of TCCN and Contrasts in an O_2-saturated 0.1 M KOH solution (scan rate: 0.5 mV s^{-1}), inset is the optical image of TCCN directly used as the OER electrode. Reproduced with permission [44]. Copyright 2016, Wiley-VCH. (e) The comparison of catalysts in onset overpotential and overpotential at 10 mA cm^{-2}. Reproduced with permission [166]. Copyright 2019, Elsevier Ltd. (f) The formation of FeNi-LDH/Ti_3C_2-MXene hybrids. (g) LSV curves of FeNi-LDH/Ti_3C_2-MXene and other catalysts. Reproduced with permission [60]. Copyright 2017, Elsevier Ltd.

Table 3. Summary of the OER performance metrics of MXene-based hybrids.

Electrocatalyst	**Electrolyte**	**$\eta_{j=10\ mA\ cm^{-2}}$ (mV)**	**Tafel slope (mV dec^{-1})**	**Ref.**
$Ti_3C_{1.6}N_{0.4}$	1.0 M KOH	~ 450	216.4	[157]
Co_3O_4/Ti_3C_2	1.0 M KOH	300	118.0	[159]
$Ti_3C_2T_x$-CoBDC	0.1 M KOH	410	48.2	[163]
Co-LDH@$Ti_3C_2T_x$	1.0 M KOH	330	82.0	[164]
CoNi LDH/$Ti_3C_2T_x$	1.0 M KOH	257.4 ($\eta_{j=100}$)	68.0	[161]
TCCN	0.1 M KOH	420	74.6	[44]
Co-B_i/Ti_3C_2	1.0 M KOH	250	53.0	[165]
CoFe-LDH/MXene	1.0 M KOH	319	50.0	[166]
FeNi-LDH/Ti_3C_2	1.0 M KOH	298	43.0	[60]
$Ti_3C_2T_x/TiO_2$/NiFeCo-LDH	0.1 M KOH	320	98.4	[168]
FeOOH NSs/Ti_3C_2	1.0 M KOH	400	95.0	[160]
S-$NiFe_2O_4$@Ti_3C_2	1.0 M KOH	270	46.8	[169]
Ru-SA/$Ti_3C_2T_x$	0.1 M $HClO_4$	290	37.9	[57]
BP QDs/ $Ti_3C_2T_x$	1.0 M KOH	360	64.3	[59]
1T/2H $MoSe_2$/MXene	1.0 M KOH	340	90.0	[170]
CoP/MXene	1.0 M KOH	230	50.0	[15]
Co/N-CNTs@$Ti_3C_2T_x$	0.1 M KOH	362	79.1	[171]

$NiCoS/Ti_3C_2T_x$	1.0 M KOH	365	58.2	[172]
$CoP@3D\text{-}Ti_3C_2$	1.0 M KOH	298	51.0	[173]
$Co_3O_4/Ti_3C_2T_x$	1.0 M KOH	340	63.97	[174]
CoP/Ti_3C_2 MXene	1.0 M KOH	280	95.4	[144]
NiFeP/MXene	1.0 M KOH	286	35.0	[167]
NiFeCe-LDH/MXene	1.0 M KOH	260	42.8	[167]
$NiCo_2O_4$/MXene	0.1 M KOH	310		[10]
N-$CoSe_2$/3D $Ti_3C_2T_x$	0.1 M KOH	310	45.0	[61]
Nitride/N-Ti_3C_2	0.1 M KOH	300	60.0	[175]
CoS_2@MXene	0.1 M KOH	270	92.0	[143]

3.1.3 Bifunctional Catalysts for Overall water splitting

The application of MXene-based catalysts in the half-reactions (HER and OER) of overall water splitting was described in 3.1.1 and 3.1.2. Due to the four-electron transfer and many reaction intermediates, OER is the rate-limiting step for the overall water splitting [5]. Therefore, the design strategy of bifunctional MXene-based catalysts is similar to that of OER. Specifically, the MXenes are preferred to be used as a substrate to construct hybrid catalysts with other active materials. With the synergy effect on electronic structure modulation, and interface or structure design, efficient overall water splitting can be achieved.

Black phosphorus quantum dots (BP QDs) expose a larger specific surface area and excellent electrocatalytic activity but suffer from the aggregation of quantum dots and poor electrical conductivity. The hybrid structure (BP QDs/MXene) obtained by van der Waals self-assembly of BP QDs and $Ti_3C_2T_x$ (MXene) significantly optimized the performance of overall water splitting [59]. MXene greatly alleviated the aggregation of BP QDs, ensuring the exposure of active sites and the accessibility of electrolytes (**Figure 8** (a)). As represented in **Figure 8** (b), theoretical calculations showed that $|\Delta G_{H^*}|$ at different active sites of the hybrids were optimized to reasonable values (0.59 and 0.17 eV) from the large negative value of $Ti_3C_2T_x$ (-1.01 eV) to the large positive value (0.81 eV) of BP QDs. Similarly, BP QDs reduced the adsorption energy of water on MXene, and obviously activated H_2O molecules, resulting in better OER performance. Therefore, BP QDs/MXene showed favorable overall water splitting performance. The overpotentials of HER and OER were only 190 mV and 360 mV at 10 mA cm^{-2} respectively. And the current density reached

up to 10 mA cm^{-2} at 1.78 V and was stable for 24 h. This strategy can also be extended to other nanoparticles. The PtPd bimetallic oxide nanoparticles loaded on $Ti_3C_2T_x$ ($PtO_aPdO_bNPs@Ti_3C_2T_x$) by solution plasma modification also showed superior performance in overall water splitting [176]. $Ti_3C_2T_x$ changed the electronic structures of Pt and Pd, which accelerated the formation of O-O bonds to reduce the barrier of proton-coupled electron transfer in OER. And the synergy significantly facilitated the rapid electrons transfer. The nanocomposite electrode demonstrated 1.53 V at the current density of 10 mA cm^{-2} and the activity attenuation was negligible (about 6 %) after 40 h testing in the alkaline electrolyte.

The heterostructure engineering between MXenes and different dimensional active materials can effectively enhance the stability and activity of the hybrids. 1T/2H $MoSe_2$/MXene heterostructure (**Figure 8** (c)) obtained by in situ one-step hydrothermal method showed high performance for efficient overall water splitting in alkaline media [170]. 1T/2H $MoSe_2$/MXene only exhibited 1.64 V at the current density of 10 m Acm^{-2} for overall water splitting (**Figure 8** (d)). MXenes significantly improved electrical conductivity and limited the aggregation of $MoSe_2$, which enhanced the charge transfer and stability of the heterostructure. It is worth noting that the 1T phase $MoSe_2$ with high conductivity and catalytic activity is usually a metastable phase, which tends to transform to the 2H phase $MoSe_2$ with poor conductivity and activity. However, after 50 hours of electrochemical testing, the structure and composition of the hybrid did not change significantly, and the content of 1T phase $MoSe_2$ only decreased from 23% to 18%. The MXene protected the metastable 1T phase $MoSe_2$ and retained more active 1T, thereby achieving increased activity and good stability. The stabilizing effect of MXene on the metastable phase is also the focus of the future material design. The hybrids formed by metal phosphides and MXene also have excellent activity [173]. Selvam *et al.* phosphated the 1D Co(OH)F nanorods grown on MXene to produce CoP/MXene with a highly mesoporous CoP array (**Figure 8** (e)) [15]. This 3D structure provided more active surfaces and boosted ions diffusion, charge transfer, and gas releasing during water splitting. As in **Figure 8** (f), the bifunctional electrode couple (CoP/MXene//CoP/MXene) exhibits better performance (1.56 V@10 mA cm^{-2}) than IrO_2/C//Pt/C (1.62 V@10 mA cm^{-2}).

Besides 0D and 1D materials, the 2D nano-sheets are also potential candidates for forming hybrid catalysts with MXenes. Yu *et al.* electrodeposited FeNi-LDHs on Ni foam coated with MXene to prepare NiFe-LDH/MXene/NF electrode [137]. This 3D electrode under alkaline conditions effectively promoted the adsorption and dissociation of water in the HER, and also improved the redox activity in the OER. Due to the activation effect, the O-H bonds of H_2O adsorbed on NiFe-LDH/MXene/NF became longer which enhanced water adsorption and dissociation, greatly accelerated the Volmer step on the electrode, prompting the HER activity. And the d-band center of Ni/Fe atoms shifted to higher energy, enhancing the O binding strength and the

redox activity of OER. In 1 M KOH, NiFe-LDH/MXene/NF could achieve a current density of 500 mA cm^{-2} at a low voltage (1.75 V vs RHE), and it steadily worked for 200 h at a current density of 100 mA cm^{-2} (**Figure 8** (g)). Du *et al.* further synthesized $Ni_xFe_{1-x}PS_3$/MXene (NFPS/MXene) hybrids through low-temperature in-situ solid-phase reaction [47]. The final NFPS showed a nano-mosaic shape instead of the original TM-LDHs nanosheets (**Figure 8** (h)). Due to the unique electronic structure of nano-mosaic and extremely high electrochemical active surface area (ECSA), NFPS/MXene exhibited excellent overall water splitting activity in 1 M KOH ($Ni_{0.9}Fe_{0.1}PS_3$@MXene: $\eta_{j=10}$ = 196 mV for HER, $Ni_{0.7}Fe_{0.3}PS_3$@MXene: $\eta_{j=10}$ = 282 mV for OER). The electrode couple assembled by $Ni_{0.9}Fe_{0.1}PS_3$@MXene and $Ni_{0.7}Fe_{0.3}PS_3$@MXene ($Ni_{0.9}Fe_{0.1}PS_3$@MXene || $Ni_{0.7}Fe_{0.3}PS_3$@MXene) showed comparable performance (1.65 V @ 10 mA cm^{-2}) to IrO_2 || Pt/C (1.71 V @ 10 mA cm^{-2}) in overall water splitting. Furthermore, as demonstrated in **Figure 8** (i), the stable operation at 1.65 V for 50 hours indicated the excellent stability of the $Ni_{0.9}Fe_{0.1}PS_3$@MXene || $Ni_{0.7}Fe_{0.3}PS_3$@MXene electrode couple. The strategy of strain engineering to adjust the electronic structure and maximize ECSA is also expected to be applied in other nanohybrids.

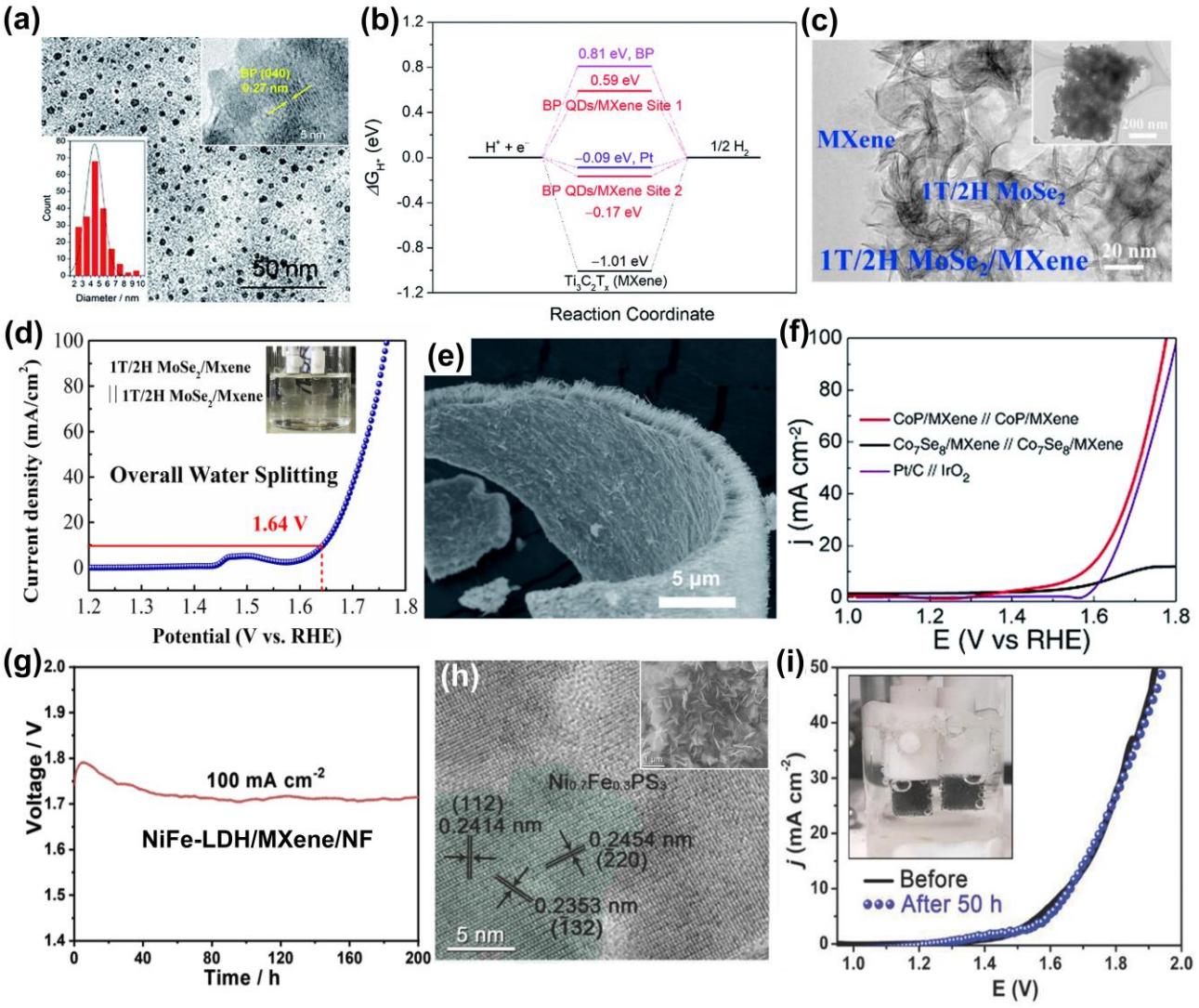

Figure 8. (a) TEM and HRTEM (inset) image of BP QDs/MXene. (b) Calculated free energy diagram (HER activity) of two adsorption sites for the BP QDs/MXene. Reproduced with permission [59]. Copyright 2018, Royal Society of Chemistry. (c) HRTEM and TEM (inset) images of 1T/2H $MoSe_2$/MXene. (d) The overall water splitting performance of 1T/2H $MoSe_2$/MXene. Reproduced with permission [170]. Copyright 2019, Elsevier Ltd. (e) SEM image of CoP/MXene. (f) The polarization curves of CoP/MXene//CoP/MXene for overall water splitting. Reproduced with permission [15]. Copyright 2019, The Royal Society of Chemistry. (g) The chronopotentiometry curve of an electrolyzer with NiFe-LDH/MXene/NF at 100 mA cm^{-2}. Reproduced with permission [137]. Copyright 2019, Elsevier Ltd. (h) HRTEM and SEM (inset) images of $Ni_{0.7}Fe_{0.3}PS_3$@MXene. (i) The LSV curves for $Ni_{0.7}Fe_{0.3}PS_3$@MXene || $Ni_{0.9}Fe_{0.1}PS_3$@MXene couple before and after the 50 h testing. Reproduced with permission [47]. Copyright 2018, WILEY-VCH.

Table 4. Summary of the Overall water splitting performance metrics of MXene-based hybrids.

Electrocatalyst	Current collector	Electrolyte	Operating Voltage (V) At 10 $mAcm^{-2}$	Ref.
BP QDs/MXene	GCE	1.0 M KOH	1.780	[59]
$PtO_aPdO_bNPs@Ti_3C_2T_x$	GCE	1.0 M KOH	1.530	[176]
1T/2H $MoSe_2$/MXene	Ni foam	1.0 M KOH	1.640	[170]
CoP/MXene	Carbon fiber paper	1.0 M KOH	1.560	[15]
CoP@3D-Ti_3C_2	Carbon paper	1.0 M KOH	1.565	[173]
NiFe-LDH/MXene	Ni foam	1.0 M KOH	1.750 at 500 $mAcm^{-2}$	[137]
$Ni_xFe_{1-x}PS_3$/MXene	GCE	1.0 M KOH	1.650	[47]
CoS_2@MXene	Ni foam	0.1 M KOH	1.630	[143]
Ti_3C_2@mNiCoP	Carbon cloth	1.0 M KOH	1.570	[177]
CoP/Ti_3C_2 MXene	RRDE	1.0 M KOH	1.578	[144]
Ni-$MoSe_2$/Ti_2NT_x	GCE	1.0 M KOH	1.590	[16]
VOOH/$Ti_3C_2T_x$ MXene	GCE	1.0 M KOH	1.579	[178]
Ru-SA/$Ti_3C_2T_x$	RDE	0.1 M $HClO_4$	1.560	[57]

In conclusion, MXene is a favorable catalyst and good support for other active materials for HER, OER, and overall water splitting. When MXenes act directly as a catalyst, the adsorption strength of reaction intermediates can be optimized by functional group adjustment, defect engineering, and heteroatom doping. As a support for active materials, MXenes provide excellent conductivity and structural support for hybrids. And due to the presence of surface functional groups, the active materials can be uniformly loaded on MXenes without aggregation and accompanied by strong coupling. It is noted that this strong coupling ensures the stability of the hybrid structure and improves its long-term cycling ability. And it also adjusts the electronic structure of the hybrids to optimize the adsorption of intermediates. Interface and structure design have always been the focus of MXene-based hybrids. A conductive 3D hybrid structure by rational design can expose more active sites and improve the mass transfer and charge transfer of the reactants, which is beneficial for the kinetic reactions.

3.2 Metal-air batteries

Besides renewable power storage, the rapidly developing electric vehicles and portable electronic devices demand better batteries, such as large energy density, high capacity, safety, and low cost [5]. Lithium-ion batteries have dominated this market in recent decades. However, they still suffer from some issues, including low energy density, high cost, and poor safety [35]. Therefore, many new rechargeable batteries have been developed, such as lithium-sulfur batteries, metal-air batteries, and so on. The metal-air batteries directly use oxygen in the air as the cathode reactant, so it has the characteristics of high energy density, low cost, and lightweight [179]. Unfortunately, metal-air batteries have not yet reached theoretical expectations due to poor air electrode activity. Specifically, the ORR/OER with slow kinetics that occurs on the air electrode severely limits the performance of the metal-air batteries [180]. Availability of efficient OER/ORR catalysts is the key to improve the performance of metal-air batteries and promote the large-scale application. Transition metal compounds have been widely studied as substitutes for noble metals, but they usually suffer from some drawbacks such as poor electrical conductivity and severe agglomeration, which seriously affect the catalytic performance [181]. MXenes as good carriers have attracted considerable attention. The excellent corrosion resistance of MXenes effectively avoids the carbon corrosion of traditional carbon supports and reduces the impact of CO_x species on the active sites during the ORR [37]. And as discussed above, MXenes can effectively reduce the aggregation of active materials and modulate the electronic structure of transition metal materials. Besides, the synergy between different components and the design of the interface and 3D structure can promote charge transfer and mass transfer to achieve the excellent catalytic activity.

The application of MXenes and hybrids in OER has been discussed in detail in chapter 3.1 (refer to 3.1.2 and 3.1.3). Therefore, this chapter mainly focuses on the applications of MXenes and hybrids as ORR and bifunctional ORR/OER catalysts. Also, the metal-air battery section mainly focuses on the very promising lithium-air batteries and zinc-air batteries, which are the most widely studied metal-air batteries. And the important performance metrics are summarized in **Table 5** and **Table 6**, respectively.

3.2.1 Catalysts for ORR

Discharging a metal-air battery is accompanied by ORR. Oxygen is reduced to H_2O or H_2O_2 through the 4-electron route without peroxide or the 2-electron route with peroxide, respectively [182]. The peroxide generated by the two-electron path may corrode the devices, and the output voltage is much lower than the four-electron path. Therefore, the four-electron path can greatly enhance the performance of the metal-air batteries. In the alkaline electrolyte, oxygen molecules are

first adsorbed on the surface of the catalysts, then the O-O bond is weakened and broken, and finally, hydroxide radicals form, accompanied by the transfer of electrons. Like OER, *HOO, *O, and *HO are also involved in ORR. The difference is that the formation of *OOH and *O affect the performance of OER, while the rate-limiting steps of ORR are the reduction steps of *OH and O_2. Therefore, it is necessary to modulate the electronic structure near the active sites for suitable adsorption strength, which optimizes its catalytic performance. Besides, hybrids interface and structural design are of importance to improve performance [153, 183, 184].

As mentioned above, the adsorption strength of oxygen-containing intermediates during the ORR is the main factor affecting the catalyst activity. The numerous hydrophilic functional groups (-OH, -F, -O) on the surface of MXenes are closely related to the adsorption of oxygen-containing intermediates. Liu *et al.* calculated the ORR performance of $Ti_{n+1}C_nT_x$ and Pt/v-$Ti_{n+1}C_nT_x$ (n=1-3, T=O and/or F, v denotes the surface vacancy) [185]. On the surface of Pt/v-$Ti_{n+1}C_nT_x$, it was found that the adsorption enthalpy of ORR intermediates was linearly related to the O/F ratio, indicating better ORR performance with more F. Similarly, the introduction of transition metal atoms on MXenes can affect the adsorption of intermediate products by modulating the electronic structure. Cu single atom catalysts on Ti_2CO_2 (Cu-Ti_2CO_2) were predicted to have excellent ORR performance [186]. The Cu atoms at the face-centered cubic (FCC) sites were more likely to adsorb and activate O_2 molecules, thereby promoting the ORR. The redistribution of charge caused by Cu atoms could improve conductivity and facilitate electron transfer, which promoted intermediates adsorption and reaction kinetics. Most importantly, this work also provided a new and simple descriptor (ξ) instead of the adsorption strength of intermediates to judge the catalytic performance of M-MXene ($\xi = \varphi_{\mathrm{M}}^{\mathrm{anchored}} \times \frac{\chi_{\mathrm{O}}^{\mathrm{ads}}}{\chi_{\mathrm{M}}^{\mathrm{anchored}} + \chi^{\mathrm{MXene}}}$, φ represents the valence electrons, χ is the electronegativity and is given by $\chi^{\mathrm{MXene}} = \frac{n_{\mathrm{M}}^{\mathrm{MXene}} \times \chi_{\mathrm{M}}^{\mathrm{MXene}} + n_{\mathrm{C(or\,N)}}^{\mathrm{MXene}} \times \chi_{\mathrm{C\,(or\,N)}}^{\mathrm{MXene}} + n_{\mathrm{O}}^{\mathrm{MXene}} \times \chi_{\mathrm{M}}^{\mathrm{MXene}}}{n_{\mathrm{M}}^{\mathrm{MXene}} + n_{\mathrm{C(or\,N)}}^{\mathrm{MXene}} + n_{\mathrm{O}}^{\mathrm{MXene}}}$, n refers to the number of elements.) (**Figure 9** (a)). The parameters involved in this descriptor were obtained from the periodic table of elements and can also be extended to other MXene-based catalysts.

Like HER and OER, MXenes also provided a broad platform for hybrids with excellent ORR performance and MXene-based hybrids were widely applied in ORR. Initially, Xie *et al.* uniformly dispersed Pt NPs on $Ti_3C_2T_2$ (T=OH, F) nanosheets to obtain the 0D/2D catalyst (Pt/$Ti_3C_2T_2$) with high activity [40]. The strong interaction between 0D Pt nanoparticles and 2D Ti_3C_2 effectively prevented the aggregation and dissolution of Pt nanoparticles, which resulted in good durability. After 10,000 cycles, the size of Pt NPs did not change significantly, nor did the ORR half-wave potential which remained at 0.847 V (while Pt/C lost 21mV) (**Figure 9** (b)). Meanwhile, the migration of electrons from the MXene led to lower-lying d-band centers (ε_d) relative to the Fermi energy (ε_F) of the Pt NPs (**Figure 9** (c)). Thus, it was easier for O_{ad} and OH_{ad} to desorb from

Pt/$Ti_3C_2T_2$, improving ORR catalytic activity. In addition to 0D nanoparticles, hybridization of 1D nanowires and 2D MXene is also a good choice. In-situ synthesized MXene-$Ag_{0.9}Ti_{0.1}$-nanowires demonstrated better activity than commercial Ag/C and pure Ag-nanowires in an alkaline medium [187]. The Ti transferred from MXene to Ag nanowire led to Ti defects in MXene, thus providing more oxygen adsorption sites. The synergistic effect of Ti and Ag in nanowires can catalyze different oxygen reduction steps and promote the four-electron transfer process. The onset potential and half-wave potential of MXene-$Ag_{0.9}Ti_{0.1}$-nanowires were 0.921 V and 0.782 V respectively. The number of electronic transfers reached 3.95.

Due to the strong coupling between the components and the special interface structure, the hybrids of 2D material and MXenes have attracted widespread attention, especially the heterostructure. A series of single-layer MXene-supported N-doped graphene heterostructures were designed based on theoretical calculations [188]. The heterostructures supported by V_2C and Mo_2C-MXenes (G/V_2C, G/Mo_2C) were preferred. The overpotentials were 0.36 V and 0.39 V for G/V_2C and G/Mo_2C, respectively. In those heterostructures, it was believed that the active center for ORR was the hollow-site C atoms near pyridine-N, and the charge redistribution caused by N doping and the electronic coupling between graphene and MXene adjusted surface binding capacity to improve ORR performance. As a classical 2D material, g-C_3N_4 can also form heterostructures with MXene for ORR [189]. The g-C_3N_4/Ti_3C_2 heterostructure exhibited improved chemisorption of O_2 due to the strong interaction between MXene and g-C_3N_4, which decreased electron density around the Ti_3C_2 sites, delivered better ORR activity and stability than commercial Pt/C. The strong synergistic effect at the interface, highly exposed atoms, and large specific surface area make the 2D/2D superlattice heterostructure widely used in electrochemistry. The Fe-N-C/MXene superlattice-like heterostructure was prepared through electrostatic self-assembly as shown in **Figure 9** (d, e) [46]. The electronic modulation caused by the synergy between MXene and Fe-N-C facilitated the adsorption of oxygen. And the strong interaction facilitated charge transfer during the reaction and improved the stability of the catalyst. The Fe-N-C/MXene heterostructure performed ORR through the 4-electrons pathway in an alkaline medium and demonstrated a low onset potential (0.92 V vs. RHE). Additionally, its half-wave potential (0.84 V) was approximately equal to the Pt/C (0.90 V) (**Figure 9** (f)). And after working for 20 hours in alkaline electrolytes, there was no significant decline in ORR activity. The interaction between MXene and Fe-N-C promoted the adsorption and reduction of oxygen at Fe-N_x sites [190, 191]. In addition to the interface, the 3D structure of the catalysts also needs to be designed. The 3D structure design of MXene-based hybrids can expose more active sites and improve the mass transfer of the reactants. To further increase the active surface, a Co-CNT/Ti_3C_2 with a 3D structure was obtained by pyrolyzing ZIF-67/Ti_3C_2 (**Figure 9** (g)) [192]. The synergy between Co nanoparticles, N-doped carbon nanotubes, and Ti_3C_2 improved

ORR performance. The rapid diffusion of O_2, numerous Co-N/C active sites, and suitable surface areas as well as highly graphitized carbon, led to comparable ORR activity to commercial Pt/C. As shown in **Figure 9** (h), Co-CNT/Ti_3C_2-60 exhibited the same half-wave potential of 0.82 V and a higher diffusion-limiting current density of 5.55 mA cm^{-2} (Pt/C, 0.82 V, 5.30 mA cm^{-2}).

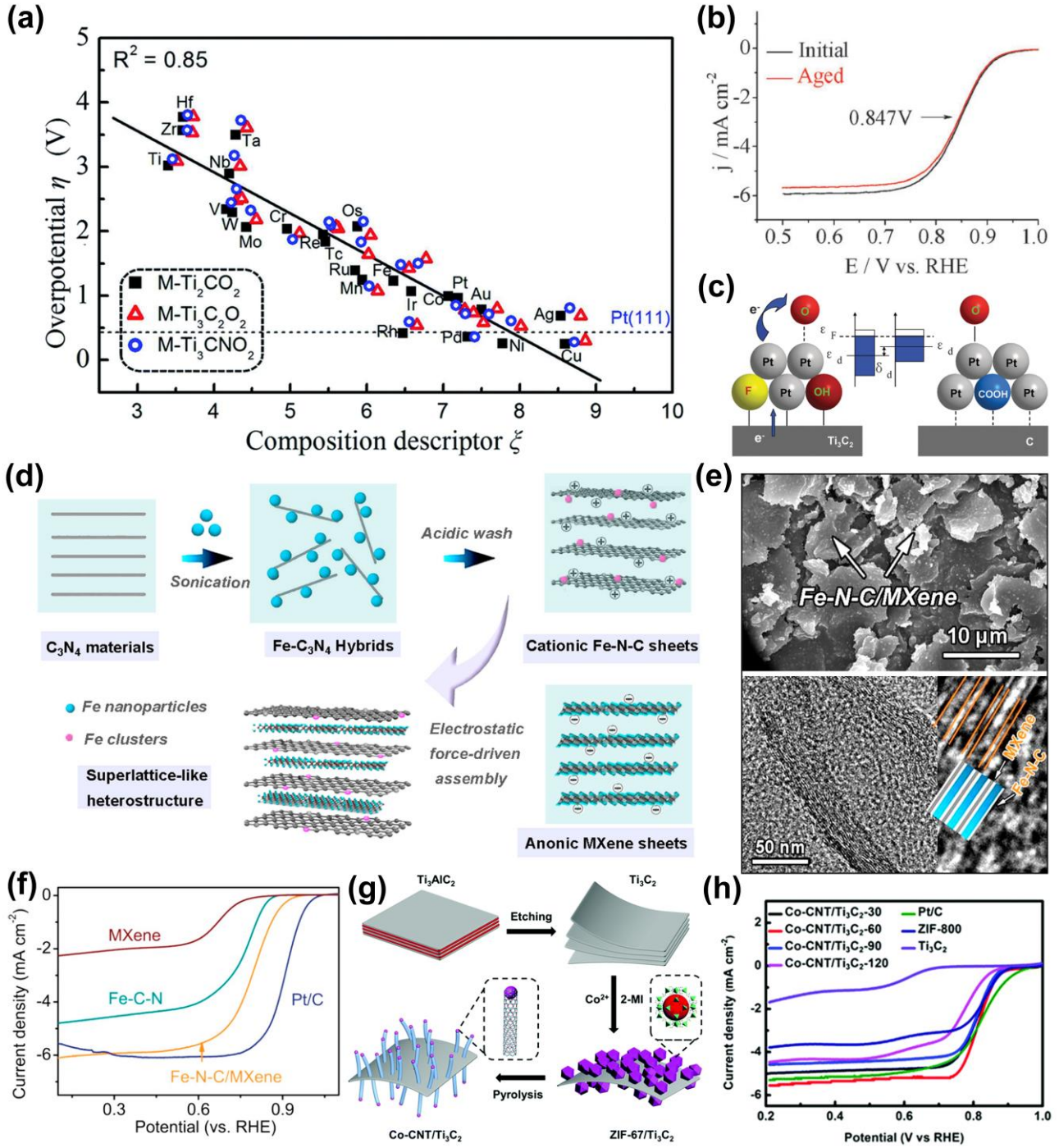

Figure 9. (a) Overpotentials versus composition descriptor ξ on M-Ti_2CO_2, M-$Ti_3C_2O_2$, and M-Ti_3CNO_2. Reproduced with permission [186]. Copyright 2019, Royal Society of Chemistry. (b) LSV curves of Pt/$Ti_3C_2X_2$. (c) Schematic description of the shift in the d-band center of the Pt/$Ti_3C_2X_2$ compared to Pt/C. Reproduced with permission [40]. Copyright 2013, Royal Society of Chemistry. (d) Schematic of the synthesis of 2D/2D Fe-N-C/MXene superlattice-like

heterostructure. (e) SEM and HRTEM image of Fe-N-C/MXene superlattice-like heterostructure. (f) LSV curves of Fe-N-C/MXene and other catalysts in 0.1 M KOH (O_2-saturated). Reproduced with permission [46]. Copyright 2020, American Chemical Society. (g) Schematic diagram of Co-CNT/Ti_3C_2 formation. (h) LSV curves of Pt/C, ZIF-800, Ti_3C_2 and Co-CNT/Ti_3C_2 in 0.1 M KOH. Reproduced with permission [192]. Copyright 2019, Royal Society of Chemistry.

Table 5. Summary of the ORR performance metrics of MXene-based hybrids.

Electrocatalyst	Electrolyte	ORR E_{onset} (V)	ORR $E_{1/2}$ (V)	N*	Ref.
$Pt/Ti_3C_2X_2$	0.1M $HClO_4$		0.847		[40]
MXene/NW-$Ag_{0.9}Ti_{0.1}$	0.1M KOH	0.921	0.782	3.95	[187]
g-C_3N_4/Ti_3C_2	0.1M KOH	0.924	0.810	3.95 - 4.05	[189]
Fe-N-C/MXene	0.1 M KOH	0.920	0.840	3.50 - 3.96	[46]
FeNC/MXene	0.1 M KOH	1.000	0.814	3.90 - 4.00	[190]
$FePc/Ti_3C_2T_x$	0.1 M KOH		0.885	~ 4.00	[191]
Fe-N-C@$Ti_3C_2T_x$	0.1 M KOH 0.1M $HClO_4$		0.887 0.777	3.80 - 4.00 3.80 - 4.00	[193]
Co-CNT/Ti_3C_2-60	0.1 M KOH		0.820	> 3.90	[192]
FeCo-N-d-$Ti_3C_2T_x$	0.1 M KOH	0.960	0.800	3.60	[194]
Co/N-CNTs@$Ti_3C_2T_x$	0.1 M KOH	0.936	0.815	3.80	[171]
$Mn_3O_4/Ti_3C_2T_x$	0.1 M KOH	0.890		~ 3.40	[195]
$NiCo_2O_4$/MXene	0.1 M KOH		0.700	3.90	[10]
N-$CoSe_2$/3D $Ti_3C_2T_x$	0.1 M KOH	0.950	0.790	3.91	[61]
Nitride/N-Ti_3C_2	0.1 M KOH	0.950	0.840	3.94	[175]
$Pt/Ti_3C_2T_x$	0.5 M H_2SO_4 0.1 M KOH	 0.950	0.772 0.853	3.13 3.71	[158]
Ru-SA/$Ti_3C_2T_x$	0.1 M $HClO_4$	0.920	0.800	3.82	[57]
MXene@PPy-800	0.1 M KOH	0.850	0.710	3.85 - 3.89	[196]
FeCo-N-d-Ti_3C_2	0.1 M KOH	0.960	0.800	3.60	[194]
MoS_2QDs@$Ti_3C_2T_x$QDs@MMWCNTs	1 M KOH	0.870	0.750	3.95	[197]

Pt/CNT-$Ti_3C_2T_x$	0.1M $HClO_4$		0.876	3.70	[198]
Ti_3C_2/NSCD-600	0.1 M KOH	0.980	0.810	3.80	[199]
CoS_2@MXene	0.1 M KOH	0.870	0.800	~ 4.00	[143]

* Number of charge transfer reactions.

3.2.2 Bifunctional catalysts for metal-air batteries

Rechargeable metal-air batteries are regarded as the next-generation energy store devices due to their high theoretical energy density [200]. OER and ORR are the core processes of charging and discharging, respectively [201]. Therefore, the efficient OER/ORR bifunctional catalysts play an important role in improving the performance of metal-air batteries. And the bifunctional catalysts based on MXenes have been widely explored. Theoretical calculation predicted that the Ti_xC_{x-1} MXenes have excellent electrocatalytic potentials as cathode catalysts for lithium-air batteries (LABs) [202-204]. Compared with the carbon materials accompanying carbon corrosion, MXenes avoid the influence of the side product (Li_2CO_3). And the good interfacial compatibility between the MXenes and Li_2O_2, coupling with the large specific surface area facilitate the continuous growth of Li_2O_2 on MXenes. Thus, the MXenes are potential high energy density cathodes for LABs.

As mentioned above, the adsorption strength of oxygen-containing intermediates during the OER/ORR is affected by the functional groups (-OH, -F, -O) on MXenes. To investigate the influence of surface groups on the performance of MXene for OER and ORR, Yang *et al.* simulated the activity of LABs by constructing adsorption models of Li_xO_2 (x=4, 2 and 1) on Ti_2C-MXene with different functional groups (non-terminated, O-terminated, F-terminated, OH-terminated) [204]. The calculation results showed that Ti_2CO_2 MXene exhibited the best catalytic activity, with the low overpotential of 0.10 V for ORR and 0.16 V for OER. It was also found that the polarization degree of Ti 3d orbital near Fermi level determined the reducibility of Ti_2C MXene, which directly affected the oxidation reaction of O_2^{2-}. Recently, Li *et al.* also obtained the same results through experiments and theoretical calculations [205]. The Ti_2C MXene nanosheets with -O and -F functional groups on the surface obtained by heat treatment were used as cathode catalysts for LABs. The discharge capacity reached 15635 mAh g^{-1} at a current density of 100 mA g^{-1}, and 250 cycles were delivered at 200 mA g^{-1} with a fixed capacity of 600 mAh g^{-1}, showing long cycle stability. The calculation results show that Ti_2CO_2 has the most suitable adsorption strength for Li_2O_2 and better catalytic performance than Ti_2CF_2 and bare Ti_2C. Besides, due to the heterogeneous surface, the discharge products mainly nucleate at the Ti_2CO_2 sites and accumulate spatially to form a porous structure during the discharge process, which effectively promotes mass transfer and cycle stability (**Figure 10** (a)). The similar mechanism also had been found in the Nb_2C with uniform O-terminated surface [206]. And the $v(e^-)$: $v(O_2)$ ratio obtained by the in-situ

differential electrochemical mass spectrometry (DEMS) was closed to 2 indicating the formation of Li_2O_2. And the Nb_2C (O-terminated) cathode exhibited excellent high-rate cycle stability (130 cycles at 3 A g^{-1}).

When applying MXenes to zinc-air batteries, the air electrode catalysts are mainly MXene-based hybrids, which is very different from lithium-air batteries. Mn_3O_4 nanoparticles loaded on Ti_3C_2 MXene demonstrated improved OER and ORR performance [195]. The metal conductivity, hydrophilicity of layered MXene, and the inhibition on particle agglomeration reduced charge transfer resistance, improved electron transfer kinetics, and ensured uniform distribution of active sites. The Zn-air battery with Mn_3O_4/MXene as the air cathode performed quite well, which showed an open-circuit voltage of 1.37 V, a battery voltage of 1.15 V under discharging current density of 20 mA cm^{-2} (close to 1.16 V with Pt/C at 20 mA cm^{-2}), a power density of up to 150 mW cm^{-2} (115 mW cm^{-2} with Pt/C). Due to the stability of the hybrid structure, the potential remained stable after a 100-hour cycle at a current density of 10 mA cm^{-2}, showing excellent stability. As expressed in **Figure 10** (b), $NiCo_2O_4$ nanocrystals in-situ anchored on MXene ($NiCo_2O_4$/MXene) can also obtain an excellent bifunctional catalyst for zinc-air batteries [10]. The XPS and NEXAFS proved the existence of Ni/Co-F bonds and synergistic effect. $NiCo_2O_4$ nanocrystals were firmly bonded to MXene by the Ni/Co-F bonds and the functional group (-F) of MXene caused the migration of Co/Ni electron clouds. The strong coupling between MXene and $NiCo_2O_4$ promoted charge transport and improved electrocatalytic activity. And the in-situ electrochemical Raman spectroscopy was employed to clarify the active sites during the OER process. The phase transition from $NiCo_2O_4$ to NiOOH and CoO_2 was observed from 1.4 V, indicating the NiOOH and CoO_2 were the active sites of $NiCo_2O_4$/MXene for OER. The aqueous zinc-air battery with $NiCo_2O_4$/MXene as cathode exhibited an ultra-high peak power density (277 mW cm^{-2}, **Figure 10** (c)), high open-circuit voltage (1.40 V), and long-term stability (over 1000 charge-discharge cycles). The flexible zinc-air battery with $NiCo_2O_4$/MXene as the air electrode also has an open-circuit voltage of 1.40 V and a high peak power density (55.1 mW cm^{-2}). Even after cutting and reconnecting, the open-circuit voltage (1.31 V) of the flexible battery is close to the initial one.

Interface design is always an efficient way to improve the catalytic performance of MXene-based hybrids. 2D transition metal nitrides have been proven to be potential OER catalysts, but with limited ORR performance. Since the M_4N structure is thermodynamically unstable, transition metal nitrides tend to form particles or thick plates. As shown in **Figure 10** (d), the hybrid NiFeMn nitride nanosheets stabilized by Ti_3C_2 nanosheets maintained the morphology of the thin plate and exposed more active sites [175]. During the annealing, some N atoms doped into the Ti_3C_2 lattice and caused the rearrangement of charges, and the coordination structure of M-N-C/Ti also formed on the interface which improved the ORR activity. XPS and XANES confirmed that Ti_3C_2 regulated the

chemical environment of metal active centers in the hybrids. Also, the aqueous zinc-air battery with this hybrid showed excellent long-term cycling stability with a high open-circuit voltage of 1.495 V and a high energy density of 693 Wh kg_{Zn}^{-1} at a current density of 10 mA cm^{-2}. Furthermore, the flexible fibrous zinc-air battery assembled with gel electrolyte also delivered an energy density of about 627 Wh kg_{Zn}^{-1} and high capacity of 570 mAh g_{Zn}^{-1}. And as demonstrated in **Figure 10** (e), the three flexible ZABs could well power blue light-emitting diode (LED) lamps in different bending states. The interface structure of the catalyst was emphasized in this work, and it also provided a new solution for improving the intrinsic activity of the material. Similarly, the aforementioned self-supporting film composed of g-C_3N_4 and Ti_3C_2 created Ti-N_x active sites through the interface design, which greatly improved the OER activity [44]. Because of its highly hydrophilic porous structure, it had been employed as a flexible oxygen electrode in zinc-air batteries. At a current density of 20 mA cm^{-2}, the charge and discharge voltages of the zinc-air battery assembled by TCCN were 2.55 V and 0.87 V, respectively, which were significantly better than IrO_2/C (2.70 V and 0.61 V). As mentioned above, the 3D structure is beneficial to mass transfer. A unique 3D N-$CoSe_2$/3D-$Ti_3C_2T_x$ structure was prepared by freeze-drying with self-assembly (**Figure 10** (f)) [61]. The increase of porosity and layer space ensured sufficient exposure of active centers and mass transfer of reactants. N-doping further reduced the energy barriers of OER and ORR. Compared with Pt/C-RuO_2-based batteries, N-$CoSe_2$/3D-MXene as air cathode in Zn-air battery delivered a higher power density of 142 mW cm^{-2} (**Figure 10** (g)) than Pt/C + RuO_2 (119 mW cm^{-2}) and ultra-long cycle life of over 500 cycles (**Figure 10** (h)).

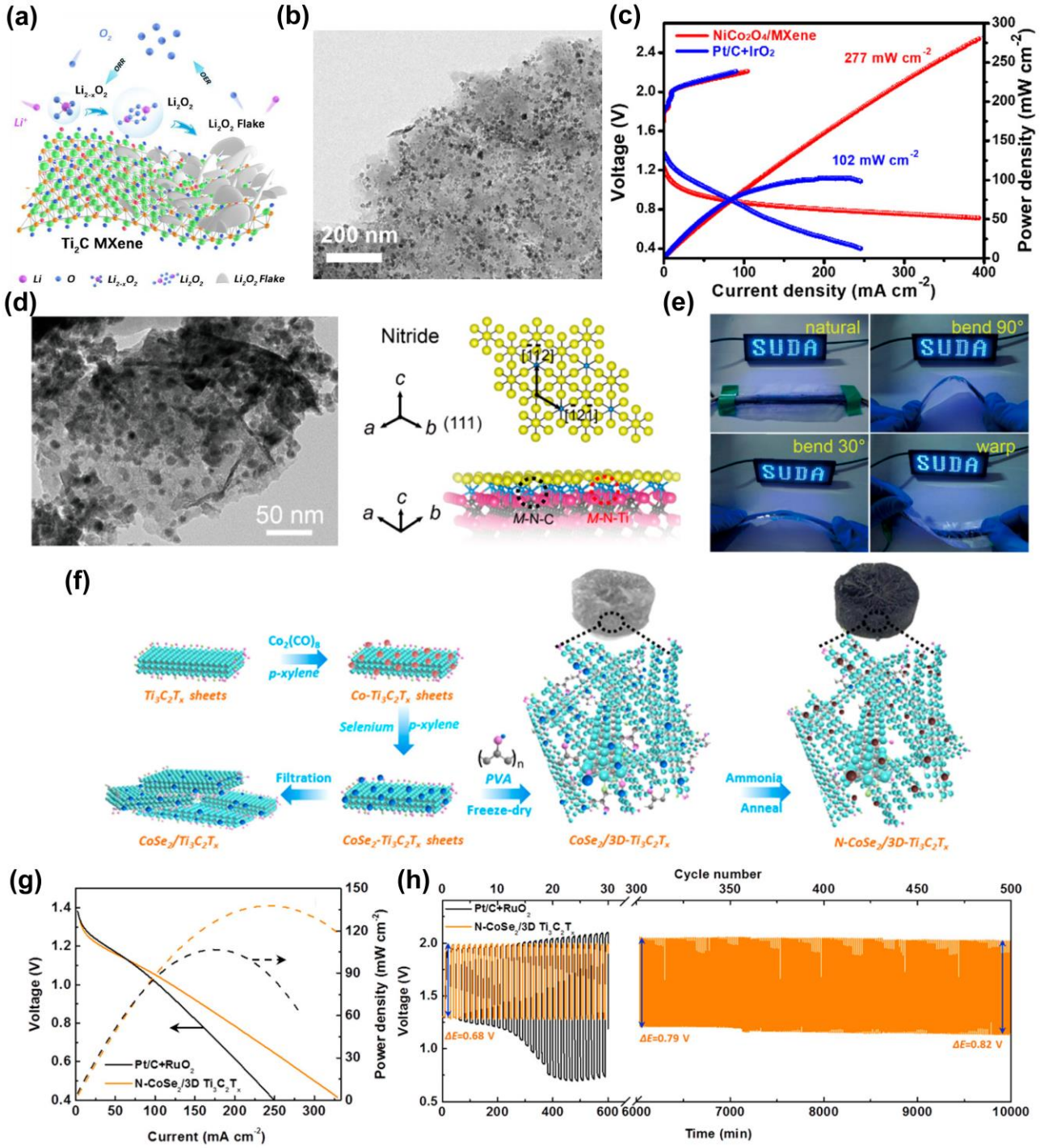

Figure 10. (a) Schematic illustration of the possible catalytic mechanism for the Ti_2C MXene under discharge/charge. Reproduced with permission [205]. Copyright 2020, Elsevier B.V. (b) TEM image of the $NiCo_2O_4$/MXene. (c) The Charge/discharge curves and power density of $NiCo_2O_4$/MXene ZAB. Reproduced with permission [10]. Copyright 2020, American Chemical Society. (d) TEM image and the corresponding structural illustrations of trimetallic nitride-Ti_3C_2 after the nitridation treatment. (e) The photos of a series-connected battery powering a blue LED (nominal voltage 3.0 V) in various bending states. Reproduced with permission [175]. Copyright 2020, American Chemical Society. (f) Schematic illustration of the synthesis of N-$CoSe_2$/3D

$Ti_3C_2T_x$. (g) The discharge curves and power density of N-$CoSe_2$/3D $Ti_3C_2T_x$ ZAB. (h) Long-term cycling performance at 10 $mAcm^{-2}$. Reproduced with permission [61]. Copyright 2019, American Chemical Society.

Table 6. Summary of the Metal-air battery performance metrics of MXene-based hybrids.

Catalyst	Substrate	Battery type	Electrolyte	Open circuit voltage (V)	Peak power density ($mW\ cm^{-2}$)	Discharge capacity ($mAh\ g^{-1}$)	Cycle stability (cycles)	Ref.
Ti_2CT_x (T=O, F)	Carbon paper	LAB (coin-type)	1 M $LiNO_3$ in DMSO			15635 at 100 mA g^{-1}	250 at 200 mA g^{-1} and 600 mAh g^{-1}	[205]
Nb_2C (O-terminated)	Carbon paper	LAB (coin-type)	1 M $LiNO_3$ in DMSO			19785.5 at 200 mA g^{-1}	130 at 3 A g^{-1} and 600 mAh g^{-1}	[206]
V-TiO_2/$Ti_3C_2T_x$	Carbon cloth	LAB (coin-type)	1 M LiTFSI in TEGDME			11487 at 100 mA g^{-1}	200 at 100 mA g^{-1} and 1000 mA h g^{-1}	[207]
Vo-SnO_2/$Ti_3C_2T_x$	Carbon cloth	LAB (coin-type)	1 M LiTFSI in TEGDME			18648 at 200 mA g^{-1}	200 at 100 mA g^{-1} and 1000 mA h g^{-1}	[208]
LaSrCoO/$Ti_3C_2T_x$	Carbon paper	LAB (coin-type)	1 M LiTFSI in EGDME			11340 at 500 mA g^{-1}	80 at 500 mA g^{-1} and 1000 mA h g^{-1}	[209]
NiO/Ti_3C_2	Carbon paper	LAB (coin-type)	1 M LiTFSI in TEGDME			13350 at 100 mA g^{-1}	90 at 500 mA g^{-1} and 500 mAh g^{-1}	[210]
CoO/$Ti_3C_2T_x$	Carbon paper	LAB (coin-type)	1 M LiTFSI in TEGDME			16220 at 100 mA g^{-1}	160 at 100 mA g^{-1} and 500 mAh g^{-1}	[211]
Ti_3C_2 QDC/N-C	Carbon paper	LAB (coin-type)	1 M LiTFSI in TEGDME			16022 at 200 mA g^{-1}	240 at 200 mA g^{-1} and 1000 mA h g^{-1}	[212]
SASe-Ti_3C_2	Carbon paper	LAB (coin-type)	1 M LiTFSI in TEGDME			17260 at 100 mA g^{-1}	170 at 200 mA g^{-1} and 1000 mA h g^{-1}	[213]
Mn_3O_4/MXene	Stainless steel mesh	liquid ZAB	6 M KOH	1.37	150			[195]
$NiCo_2O_4$/MXene	Nickel foam	liquid ZAB	6 M KOH + 0.2 M $Zn(AC)_2$	1.40	277	768.6 mA h g^{-1} at 10 mA cm^{-2}	1000 at 5 mA cm^{-2}	[10]
		flexible ZAB	KOH/PVA	1.40	55.1		100 at 1 mA cm^{-2}	
Nitride/N-Ti_3C_2	Carbon cloth	liquid ZAB	6 M KOH + 0.2 M $Zn(AC)_2$	1.495		630 mAh g_{Zn}^{-1} at 10 mA cm^{-2}	120 at 20 mA cm^{-2}	[175]
		fiber-shaped flexible ZAB	KOH/PVA	1.325		570 mAh g_{Zn}^{-1} at 5 mA cm^{-3}		

TCCN	Free-standing film	liquid ZAB (coin-type)	6 M KOH				15 at 20 mA cm^{-2}	[44]
N-$CoSe_2$/3D $Ti_3C_2T_x$	Carbon paper	liquid ZAB	6 M KOH + 2 M $ZnCl_2$	1.43	142	751 mAh g_{Zn}^{-1} at 5 mA cm^{-2}	500 at 10 mA cm^{-2}	[61]
CoS_2@MXene	Carbon cloth	flexible ZAB	KOH/PAA	1.46	29		60 at 1 mA cm^{-2}	[143]
LDH/MQDs/NG	Carbon cloth	liquid ZAB flexible ZAB	6 M KOH + 0.2 M $Zn(AC)_2$ KOH/PVA/$ZnCl_2$	1.42	113.8 57.6	598 mAh g_{Zn}^{-1} at 5 mA cm^{-2}	900 at 5 mA cm^{-2}	[214]
$H_2PO_2^-$ /FeNi-LDH-V_2C	Carbon paper	liquid ZAB	6 M KOH + 0.2 M $Zn(AC)_2$	1.42	137		600 at 5 mA cm^{-2}	[215]

In this part, the application of MXenes and hybrids in ORR and metal-air batteries was presented. The regulation of MXene functional groups and heteroatoms doping have been proved to be effective strategies to optimize the adsorption of intermediate products, leading to better ORR activity. Among the MXene-based ORR catalysts, the research of coupling MXenes with other materials is the most extensive. With the strong coupling between hybrids, 0D, 1D, and 2D materials can be uniformly and firmly loaded on MXenes. The synergistic effect between the components is of importance to improving performance. The unique heterostructure and interface formed between 2D materials and MXenes are also worth noting. Proper interface design can create new ORR active sites, modulate the electronic structure, and facilitate the adsorption of oxygen. Also, the design of the three-dimensional structure is beneficial to ORR with the slow kinetic reaction, because of more exposed active sites and promoted mass/charge transfer. For the bifunctional catalysts in metal-air batteries, related research on MXenes and their hybrids mainly focuses on lithium-air batteries and zinc-air batteries. Due to the theoretically suitable adsorption capacity of Li-related species, MXenes are considered to be a potential high-efficiency catalyst for lithium-air batteries. The synergy between MXenes and active materials has been widely utilized in the development of air electrode catalysts. The change in electronic structure caused by strong coupling is the key to achieving excellent bifunctional activity. Furthermore, a three-dimensional structure of MXene-based hybrids was also chosen, which is conducive to the mass diffusion and charge transfer of the reactants on the air electrode. In addition, with the development of portable electronic devices, flexible metal-air batteries also demonstrate broad application prospects. And the membrane electrodes prepared by MXenes show excellent flexibility and mechanical properties, which have been widely used in flexible supercapacitors and other fields. Therefore, MXene-based

self-supporting flexible film electrodes may greatly promote the development of flexible metal-air batteries. It is noted that the electrochemical performances and energy density of the flexible metal-air batteries need further development, and the rational cathodes, especially the light and highly active MXene based catalysts may be the key to accelerate the commercial application.

4 Summary and perspective

In this review, we systematically introduced the application of MXenes in HER, OER, overall water splitting, ORR, and metal-air batteries. MXenes as catalysts and support agents have great potential for electrocatalysis applications. Surface functional group adjustment, defects control, heteroatoms doping, and other methods can optimize the electronic structure of MXenes and thus their electrocatalysis activity. MXene-based hybrids with rationally designed structures can exposure more active sites and facilitate mass transfer, and thus also prove to be effective to achieve the higher activity.

Although many breakthroughs have been achieved, there are still many challenges in the application of MXene-based materials in electrocatalysis. (1) Exploring the compositional space of MXenes is of significance. Numerous MXenes have been theoretically proved to be stable, but only a few of them have been successfully prepared, resulting in that most studies are limited to several common MXenes (e.g., Ti_3C_2, Ti_2C, and Mo_2C). (2) Although the etching method makes MXenes feasible for large-scale preparation, it is still difficult to prepare MXenes nanosheets with uniform and large size. In addition, the design of the container and the environmental issues caused by HF during the large-scale preparation should also be considered. (3) MXenes are easily oxidized in water and air, and the changes of storage conditions (low temperature, organic solvents) and the use of additives are not satisfactory. How to improve the stability of MXene is critical for their practical applications. (4) Due to the influence of multiple factors such as the diversity of MXene composition, functional groups, defects, and so on, the improvement of MXene performance in different fields lacks a clear direction. (5) Although construction of 3D structure is a general strategy to improve MXene based catalytic activity, the accurate control of the structure needs further development. (6) The in-situ characterization techniques may be introduced to understand the specific reaction mechanisms and further clarify the catalysis mechanism of MXenes. (7) The development of flexible self-supporting film electrodes based on MXenes are conducive to flexible wearable energy storage or conversion devices such as flexible metal-air batteries and flexible supercapacitors. How to balance the structural design and flexibility is still a challenge.

Compared with other 2D materials, MXenes can be synthesized using a scalable etching method, implying promise for commercial products. As described above, more attention is paid to

MXene-based electrocatalysis, and a number of articles on MXenes enlarge their applications, such as electromagnetic shielding, energy storage, water purification, and so on. But the fundamental properties should be more concerned, especially the mechanism of the reactions, origin of those functionality, and accurate control strategies for electrocatalysis. Overcoming these fundamental issues and targeting appropriate electrochemical catalysis are central to the commercialization of MXenes. Only with great application potential, the discussion about the safety, material abundance, or cost is meaningful.

References

[1] T. Zhou, W. Xu, N. Zhang, Z. Du, C. Zhong, W. Yan, H. Ju, W. Chu, H. Jiang, C. Wu, Y. Xie, Ultrathin Cobalt Oxide Layers as Electrocatalysts for High-Performance Flexible Zn-Air Batteries, Adv. Mater. 31 (2019) 1807468. https://doi.org/10.1002/adma.201807468.

[2] K. Zhu, J. Chen, W. Wang, J. Liao, J. Dong, M.O.L. Chee, N. Wang, P. Dong, P.M. Ajayan, S. Gao, J. Shen, M. Ye, Etching-Doping Sedimentation Equilibrium Strategy: Accelerating Kinetics on Hollow Rh-Doped CoFe-Layered Double Hydroxides for Water Splitting, Adv. Funct. Mater. 30 (2020) 2003556. https://doi.org/10.1002/adfm.202003556.

[3] Y. Yang, S. Bremner, C. Menictas, M. Kay, Battery energy storage system size determination in renewable energy systems: A review, Renew. Sust. Energ. Rev. 91 (2018) 109-125. https://doi.org/10.1016/j.rser.2018.03.047.

[4] N. Mahmud, A. Zahedi, Review of control strategies for voltage regulation of the smart distribution network with high penetration of renewable distributed generation, Renew. Sust. Energ. Rev. 64 (2016) 582-595. https://doi.org/10.1016/j.rser.2016.06.030.

[5] S. Wang, S. Chen, L. Ma, J.A. Zapien, Recent Progress in Cobalt-based Carbon Materials as Oxygen Electrocatalysts for Zinc-Air Batteries Applications, Mater. Today Energy 20 (2021) 100659. https://doi.org/10.1016/j.mtener.2021.100659.

[6] T. Zhu, S. Liu, B. Huang, Q. Shao, M. Wang, F. Li, X. Tan, Y. Pi, S.-C. Weng, B. Huang, Z. Hu, J. Wu, Y. Qian, X. Huang, High-performance diluted nickel nanoclusters decorating ruthenium nanowires for pH-universal overall water splitting, Energy Environ. Sci. 14 (2021) 3194-3202. https://doi.org/10.1039/d0ee04028b.

[7] Z. Wang, X. Yao, Y. Kang, L. Miao, D. Xia, L. Gan, Structurally Ordered Low-Pt Intermetallic Electrocatalysts toward Durably High Oxygen Reduction Reaction Activity, Adv. Funct. Mater. 29 (2019) 1902987. https://doi.org/10.1002/adfm.201902987.

[8] Y.Z. Wen, T. Yang, C.Q. Cheng, X.R. Zhao, E.Z. Liu, J. Yang, Engineering Ru(IV) charge density in Ru@RuO_2 core-shell electrocatalyst via tensile strain for efficient oxygen evolution in acidic media, Chin. J. Catal. 41 (2020) 1161-1167. https://doi.org/10.1016/s1872-2067(20)63543-4.

[9] Y. Tian, X. Liu, L. Xu, D. Yuan, Y. Dou, J. Qiu, H. Li, J. Ma, Y. Wang, D. Su, S. Zhang, Engineering Crystallinity and Oxygen Vacancies of Co(II) Oxide Nanosheets for High Performance and Robust Rechargeable Zn-Air Batteries, Adv. Funct. Mater. 31 (2021) 2101239. https://doi.org/10.1002/adfm.202101239.

[10] H. Lei, S. Tan, L. Ma, Y. Liu, Y. Liang, M.S. Javed, Z. Wang, Z. Zhu, W. Mai, Strongly Coupled $NiCo_2O_4$ Nanocrystal/MXene Hybrid through In Situ Ni/Co-F Bonds for Efficient Wearable Zn-Air Batteries, ACS Appl. Mater. Interfaces 12 (2020) 44639-44647. https://doi.org/10.1021/acsami.0c11185.

[11] D. Chen, X. Chen, Z. Cui, G. Li, B. Han, Q. Zhang, J. Sui, H. Dong, J. Yu, L. Yu, L. Dong, Dual-active-site hierarchical architecture containing NiFe-LDH and ZIF-derived carbon-based framework composite as efficient bifunctional oxygen electrocatalysts for durable rechargeable Zn-air batteries, Chem. Eng. J. 399 (2020) 125718. https://doi.org/10.1016/j.cej.2020.125718.

[12] H. Sun, W. Zhang, J.-G. Li, Z. Li, X. Ao, K.-H. Xue, K.K. Ostrikov, J. Tang, C. Wang, Rh-engineered ultrathin NiFe-LDH nanosheets enable highly-efficient overall water splitting and urea electrolysis, Appl. Catal. B Environ. 284 (2021) 119740. https://doi.org/10.1016/j.apcatb.2020.119740.

[13] S. Bolar, S. Shit, J.S. Kumar, N.C. Murmu, R.S. Ganesh, H. Inokawa, T. Kuila, Optimization of active surface area of flower like MoS_2 using V-doping towards enhanced hydrogen evolution reaction in acidic and basic medium, Appl. Catal. B Environ. 254 (2019) 432-442. https://doi.org/10.1016/j.apcatb.2019.04.028.

[14] P. Kuang, M. He, B. Zhu, J. Yu, K. Fan, M. Jaroniec, 0D/2D NiS_2/V-MXene composite for electrocatalytic H_2 evolution, J. Catal. 375 (2019) 8-20. https://doi.org/10.1016/j.jcat.2019.05.019.

[15] N.C.S. Selvam, J. Lee, G.H. Choi, M.J. Oh, S. Xu, B. Lim, P.J. Yoo, MXene supported Co_xA_y (A = OH, P, Se) electrocatalysts for overall water splitting: unveiling the role of anions in intrinsic activity and stability, J. Mater. Chem. A 7 (2019) 27383-27393. https://doi.org/10.1039/c9ta10664b.

[16] H. Zong, K. Yu, Z. Zhu, Heterostructure nanohybrids of Ni-doped $MoSe_2$ coupled with Ti_2NT_x toward efficient overall water splitting, Electrochim. Acta 353 (2020) 136598. https://doi.org/10.1016/j.electacta.2020.136598.

[17] H. Yu, L. Shang, T. Bian, R. Shi, G.I.N. Waterhouse, Y. Zhao, C. Zhou, L.-Z. Wu, C.-H. Tung, T. Zhang, Nitrogen-Doped Porous Carbon Nanosheets Templated from g-C_3N_4 as Metal-Free Electrocatalysts for Efficient Oxygen Reduction Reaction, Adv. Mater. 28 (2016) 5080-5086. https://doi.org/10.1002/adma.201600398.

[18] C.L. Tan, X.H. Cao, X.J. Wu, Q.Y. He, J. Yang, X. Zhang, J.Z. Chen, W. Zhao, S.K. Han, G.H. Nam, M. Sindoro, H. Zhang, Recent Advances in Ultrathin Two-Dimensional Nanomaterials, Chem. Rev. 117 (2017) 6225-6331. https://doi.org/10.1021/acs.chemrev.6b00558.

[19] J. Zhu, Z.-C. Wang, H. Dai, Q. Wang, R. Yang, H. Yu, M. Liao, J. Zhang, W. Chen, Z. Wei, N. Li, L. Du, D. Shi, W. Wang, L. Zhang, Y. Jiang, G. Zhang, Boundary activated hydrogen evolution reaction on monolayer MoS_2, Nat. Commun. 10 (2019) 1348. https://doi.org/10.1038/s41467-019-09269-9.

[20] X. Ren, J. Zhou, X. Qi, Y. Liu, Z. Huang, Z. Li, Y. Ge, S.C. Dhanabalan, J.S. Ponraj, S. Wang, J. Zhong, H. Zhang, Few-Layer Black Phosphorus Nanosheets as Electrocatalysts for Highly Efficient Oxygen Evolution Reaction, Adv. Energy Mater. 7 (2017) 1700396. https://doi.org/10.1002/aenm.201700396.

[21] L. Yu, J.F. Yang, B.Y. Guan, Y. Lu, X.W. Lou, Hierarchical Hollow Nanoprisms Based on Ultrathin Ni-Fe Layered Double Hydroxide Nanosheets with Enhanced Electrocatalytic Activity towards Oxygen Evolution, Angew. Chem. Int. Ed. 57 (2018) 172-176. https://doi.org/10.1002/anie.201710877.

[22] X. Chia, M. Pumera, Characteristics and performance of two-dimensional materials for electrocatalysis, Nat. Catal. 1 (2018) 909-921. https://doi.org/10.1038/s41929-018-0181-7.

[23] K. Khan, A.K. Tareen, M. Aslam, Y.P. Zhang, R.H. Wang, Z.B. Ouyang, Z.Y. Gou, H. Zhang, Recent advances in two-dimensional materials and their nanocomposites in sustainable energy conversion applications, Nanoscale 11 (2019) 21622-21678. https://doi.org/10.1039/c9nr05919a.

[24] J. Liu, C. Guo, A. Vasileff, S. Qiao, Nanostructured 2D Materials: Prospective Catalysts for Electrochemical CO_2 Reduction, Small Methods 1 (2017) 1600006. https://doi.org/10.1002/smtd.201600006.

[25] Z.Y. Wang, F.F. Zhang, H.Y. Zou, Y.H. Yuan, H.Y. Wang, J.F. Xia, Z.H. Wang, Preparation of a Pt/NiFe layered double hydroxide/reduced graphene oxide composite as an electrocatalyst for methanol oxidation, J. Electroanal. Chem. 818 (2018) 198-203. https://doi.org/10.1016/j.jelechem.2018.04.046.

[26] B.S. Li, C. Lai, M.M. Zhang, G.M. Zeng, S.Y. Liu, D.L. Huang, L. Qin, X.G. Liu, H. Yi, F.H. Xu, N. An, L. Chen, Graphdiyne: A Rising Star of Electrocatalyst Support for Energy Conversion, Adv. Energy Mater. 10 (2020) 25. https://doi.org/10.1002/aenm.202000177.

[27] B. Huang, N. Zhou, X. Chen, W.J. Ong, N. Li, Insights into the Electrocatalytic Hydrogen Evolution Reaction Mechanism on Two-Dimensional Transition-Metal Carbonitrides (MXene), Chem. Eur. J. 24 (2018) 18479-18486. https://doi.org/10.1002/chem.201804686.

[28] G. Gao, A.P. O'Mullane, A. Du, 2D MXenes: A New Family of Promising Catalysts for the Hydrogen Evolution Reaction, ACS Catal. 7 (2016) 494-500. https://doi.org/10.1021/acscatal.6b02754.

[29] M. Naguib, M. Kurtoglu, V. Presser, J. Lu, J. Niu, M. Heon, L. Hultman, Y. Gogotsi, M.W. Barsoum, Two-dimensional nanocrystals produced by exfoliation of Ti_3AlC_2, Adv. Mater. 23 (2011) 4248-4253. https://doi.org/10.1002/adma.201102306.

[30] M. Naguib, V.N. Mochalin, M.W. Barsoum, Y. Gogotsi, 25th anniversary article: MXenes: a new family of two-dimensional materials, Adv. Mater. 26 (2014) 992-1005. https://doi.org/10.1002/adma.201304138.

[31] B. Anasori, M.R. Lukatskaya, Y. Gogotsi, 2D metal carbides and nitrides (MXenes) for energy storage, Nat. Rev. Mater. 2 (2017) 16098. https://doi.org/10.1038/natrevmats.2016.98.

[32] B. Anasori, Y. Xie, M. Beidaghi, J. Lu, B.C. Hosler, L. Hultman, P.R.C. Kent, Y. Gogotsi, M.W. Barsoum, Two-Dimensional, Ordered, Double Transition Metals Carbides (MXenes), ACS Nano 9 (2015) 9507-9516. https://doi.org/10.1021/acsnano.5b03591.

[33] N.C. Frey, J. Wang, G.I. Vega Bellido, B. Anasori, Y. Gogotsi, V.B. Shenoy, Prediction of Synthesis of 2D Metal Carbides and Nitrides (MXenes) and Their Precursors with Positive and Unlabeled Machine Learning, ACS Nano 13 (2019) 3031-3041. https://doi.org/10.1021/acsnano.8b08014.

[34] J. Sui, X. Chen, Y. Li, W. Peng, F. Zhang, X. Fan, MXene derivatives: synthesis and applications in energy convention and storage, RSC Adv. 11 (2021) 16065-16082. https://doi.org/10.1039/d0ra10018h.

[35] Y. Dong, H. Shi, Z.S. Wu, Recent Advances and Promise of MXene- Based Nanostructures for High-Performance Metal Ion Batteries, Adv. Funct. Mater. 30 (2020) 2000706. https://doi.org/10.1002/adfm.202000706.

[36] J. Xie, J. Qi, F. Lei, Y. Xie, Modulation of electronic structures in two-dimensional electrocatalysts for hydrogen evolution reaction, Chem. Commun. 56 (2020) 11910-11930. https://doi.org/10.1039/d0cc05272h.

[37] S.G. Peera, C. Liu, J. Shim, A.K. Sahu, T.G. Lee, M. Selvaraj, R. Koutavarapu, MXene ($Ti_3C_2T_x$) supported electrocatalysts for methanol and ethanol electrooxidation: A review, Ceram.Int. (2021) in press. https://doi.org/10.1016/j.ceramint.2021.07.075.

[38] J. Zhao, Z. Tu, S.H. Chan, Carbon corrosion mechanism and mitigation strategies in a proton exchange membrane fuel cell (PEMFC): A review, J. Power Sources 488 (2021) 229434. https://doi.org/10.1016/j.jpowsour.2020.229434.

[39] K. Li, M. Liang, H. Wang, X. Wang, Y. Huang, J. Coelho, S. Pinilla, Y. Zhang, F. Qi, V. Nicolosi, Y. Xu, 3D MXene Architectures for Efficient Energy Storage and Conversion, Adv. Funct. Mater. 30 (2020) 2000842. https://doi.org/10.1002/adfm.202000842.

[40] X. Xie, S. Chen, W. Ding, Y. Nie, Z. Wei, An extraordinarily stable catalyst: Pt NPs supported on two-dimensional $Ti_3C_2X_2$ (X = OH, F) nanosheets for oxygen reduction reaction, Chem. Commun. 49 (2013) 10112-10114. https://doi.org/10.1039/c3cc44428g.

[41] D. Kan, D. Wang, X. Zhang, R. Lian, J. Xu, G. Chen, Y. Wei, Rational design of bifunctional ORR/OER catalysts based on Pt/Pd-doped Nb_2CT_2 MXene by first-principles calculations, J. Mater. Chem. A 8 (2020) 3097-3108. https://doi.org/10.1039/c9ta12255a.

[42] Z. Li, Y. Cui, Z. Wu, C. Milligan, L. Zhou, G. Mitchell, B. Xu, E. Shi, J.T. Miller, F.H. Ribeiro, Y. Wu, Reactive metal-support interactions at moderate temperature in two-dimensional niobium-carbide-supported platinum catalysts, Nat. Catal. 1 (2018) 349-355. https://doi.org/10.1038/s41929-018-0067-8.

[43] Z.W. Seh, K.D. Fredrickson, B. Anasori, J. Kibsgaard, A.L. Strickler, M.R. Lukatskaya, Y. Gogotsi, T.F. Jaramillo, A. Vojvodic, Two-Dimensional Molybdenum Carbide (MXene) as an Efficient Electrocatalyst for Hydrogen Evolution, ACS Energy Lett. 1 (2016) 589-594. https://doi.org/10.1021/acsenergylett.6b00247.

[44] T.Y. Ma, J.L. Cao, M. Jaroniec, S.Z. Qiao, Interacting Carbon Nitride and Titanium Carbide Nanosheets for High-Performance Oxygen Evolution, Angew. Chem. Int. Ed. 55 (2016) 1138-1142. https://doi.org/10.1002/anie.201509758.

[45] J. Zhang, Y. Zhao, X. Guo, C. Chen, C.-L. Dong, R.-S. Liu, C.-P. Han, Y. Li, Y. Gogotsi, G. Wang, Single platinum atoms immobilized on an MXene as an efficient catalyst for the hydrogen evolution reaction, Nat. Catal. 1 (2018) 985-992. https://doi.org/10.1038/s41929-018-0195-1.

[46] L. Jiang, J. Duan, J. Zhu, S. Chen, M. Antonietti, Iron Clusters-Directed Synthesis of 2D/2D Fe-N-C/MXene SuperlatticeLike Heterostructure with Enhanced Oxygen Reduction Electrocatalysis, ACS Nano 14 (2020) 2436-2444. https://doi.org/10.1021/acsnano.9b09912.

[47] C.-F. Du, K.N. Dinh, Q. Liang, Y. Zheng, Y. Luo, J. Zhang, Q. Yan, Self-Assemble and In Situ Formation of $Ni_{1-x}Fe_xPS_3$ Nanomosaic-Decorated MXene Hybrids for Overall Water Splitting, Adv. Energy Mater. 8 (2018) 1801127. https://doi.org/10.1002/aenm.201801127.

[48] T.P. Nguyen, D.M. Tuan Nguyen, D.L. Tran, H.K. Le, D.-V.N. Vo, S.S. Lam, R.S. Varma, M. Shokouhimehr, C.C. Nguyen, Q.V. Le, MXenes: Applications in electrocatalytic, photocatalytic hydrogen evolution reaction and CO_2 reduction, Mol. Catal. 486 (2020) 110850. https://doi.org/10.1016/j.mcat.2020.110850.

[49] J. Peng, X. Chen, W.-J. Ong, X. Zhao, N. Li, Surface and Heterointerface Engineering of 2D MXenes and Their Nanocomposites: Insights into Electro- and Photocatalysis, Chem 5 (2019) 18-50. https://doi.org/10.1016/j.chempr.2018.08.037.

[50] A. Zhang, R. Liu, J. Tian, W. Huang, J. Liu, MXene-Based Nanocomposites for Energy Conversion and Storage Applications, Chem. Eur. J. 26 (2020) 6342-6359. https://doi.org/10.1002/chem.202000191.

[51] J. Luo, E. Matios, H. Wang, X. Tao, W. Li, Interfacial structure design of MXene- based nanomaterials for electrochemical energy storage and conversion, InfoMat 2 (2020) 1057-1076. https://doi.org/10.1002/inf2.12118.

[52] H. Wang, J.-M. Lee, Recent advances in structural engineering of MXene electrocatalysts, J. Mater. Chem. A 8 (2020) 10604-10624. https://doi.org/10.1039/d0ta03271a.

[53] A. Liu, X. Liang, X. Ren, W. Guan, M. Gao, Y. Yang, Q. Yang, L. Gao, Y. Li, T. Ma, Recent Progress in MXene-Based Materials: Potential High- Performance Electrocatalysts, Adv. Funct. Mater. 30 (2020) 2003437. https://doi.org/10.1002/adfm.202003437.

[54] Y. Gogotsi, B. Anasori, The Rise of MXenes, ACS Nano 13 (2019) 8491-8494. https://doi.org/10.1021/acsnano.9b06394.

[55] J. Xia, S. Yang, B. Wang, P. Wu, I. Popovs, H. Li, S. Irle, S. Dai, H. Zhu, Boosting Electrosynthesis of Ammonia on Surface-Engineered MXene Ti_3C_2, Nano Energy 72 (2020) 104681. https://doi.org/10.1016/j.nanoen.2020.104681.

[56] G. Qu, Y. Zhou, T. Wu, G. Zhao, F. Li, Y. Kang, C. Xu, Phosphorized MXene-Phase Molybdenum Carbide as an Earth-Abundant Hydrogen Evolution Electrocatalyst, ACS Appl. Energy Mater. 1 (2018) 7206-7212. https://doi.org/10.1021/acsaem.8b01642.

[57] X. Peng, S. Zhao, Y. Mi, L. Han, X. Liu, D. Qi, J. Sun, Y. Liu, H. Bao, L. Zhuo, H.L. Xin, J. Luo, X. Sun, Trifunctional Single-Atomic Ru Sites Enable Efficient Overall Water Splitting and Oxygen Reduction in Acidic Media, Small 16 (2020) 2002888. https://doi.org/10.1002/smll.202002888.

[58] X. Sang, Y. Xie, M.W. Lin, M. Alhabeb, K.L. Van Aken, Y. Gogotsi, P.R.C. Kent, K. Xiao, R.R. Unocic, Atomic Defects in Monolayer Titanium Carbide ($Ti_3C_2T_x$) MXene, ACS Nano 10 (2016) 9193-9200. https://doi.org/10.1021/acsnano.6b05240.

[59] X.-D. Zhu, Y. Xie, Y.-T. Liu, Exploring the synergy of 2D MXene-supported black phosphorus quantum dots in hydrogen and oxygen evolution reactions, J. Mater. Chem. A 6 (2018) 21255-21260. https://doi.org/10.1039/c8ta08374f.

[60] M. Yu, S. Zhou, Z. Wang, J. Zhao, J. Qiu, Boosting electrocatalytic oxygen evolution by synergistically coupling layered double hydroxide with MXene, Nano Energy 44 (2018) 181-190. https://doi.org/10.1016/j.nanoen.2017.12.003.

[61] Z. Zeng, G. Fu, H.B. Yang, Y. Yan, J. Chen, Z. Yu, J. Gao, L.Y. Gan, B. Liu, P. Chen, Bifunctional N‐$CoSe_2$/3D-MXene as Highly Efficient and Durable Cathode for Rechargeable Zn-Air Battery, ACS Mater. Lett. 1 (2019) 432-439. https://doi.org/10.1021/acsmaterialslett.9b00337.

[62] Y. Gao, Y. Cao, H. Zhuo, X. Sun, Y. Gu, G. Zhuang, S. Deng, X. Zhong, Z. Wei, X. Li, J.-g. Wang, Mo_2TiC_2 MXene: A Promising Catalyst for Electrocatalytic Ammonia Synthesis, Catal. Today 339 (2020) 120-126. https://doi.org/10.1016/j.cattod.2018.12.029.

[63] M. Ghidiu, M. Naguib, C. Shi, O. Mashtalir, L.M. Pan, B. Zhang, J. Yang, Y. Gogotsi, S.J. Billinge, M.W. Barsoum, Synthesis and characterization of two-dimensional Nb_4C_3 (MXene), Chem. Commun. 50 (2014) 9517-9520. https://doi.org/10.1039/c4cc03366c.

[64] M. Naguib, V. Presser, D. Tallman, J. Lu, L. Hultman, Y. Gogotsi, M.W. Barsoum, On the Topotactic Transformation of Ti_2AlC into a Ti-C-O-F Cubic Phase by Heating in Molten Lithium Fluoride in Air, J. Am. Ceram. Soc. 94 (2011) 4556-4561. https://doi.org/10.1111/j.1551-2916.2011.04896.x.

[65] M. Ghidiu, M.R. Lukatskaya, M.Q. Zhao, Y. Gogotsi, M.W. Barsoum, Conductive two-dimensional titanium carbide 'clay' with high volumetric capacitance, Nature 516 (2014) 78-81. https://doi.org/10.1038/nature13970.

[66] X. Zou, H. Liu, H. Xu, X. Wu, X. Han, J. Kang, K.M. Reddy, A simple approach to synthesis Cr_2CT_x MXene for efficient hydrogen evolution reaction, Mater. Today Energy 20 (2021) 100668. https://doi.org/10.1016/j.mtener.2021.100668.

[67] J. Halim, M.R. Lukatskaya, K.M. Cook, J. Lu, C.R. Smith, L.A. Naslund, S.J. May, L. Hultman, Y. Gogotsi, P. Eklund, M.W. Barsoum, Transparent Conductive Two-Dimensional Titanium Carbide Epitaxial Thin Films, Chem. Mater. 26 (2014) 2374-2381. https://doi.org/10.1021/cm500641a.

[68] P. Urbankowski, B. Anasori, T. Makaryan, D. Er, S. Kota, P.L. Walsh, M. Zhao, V.B. Shenoy, M.W. Barsoum, Y. Gogotsi, Synthesis of two-dimensional titanium nitride Ti_4N_3 (MXene), Nanoscale 8 (2016) 11385-11391. https://doi.org/10.1039/c6nr02253g.

[69] T. Li, L. Yao, Q. Liu, J. Gu, R. Luo, J. Li, X. Yan, W. Wang, P. Liu, B. Chen, W. Zhang, W. Abbas, a. Naz, D. Zhang, Fluorine-Free Synthesis of High-Purity $Ti_3C_2T_x$ (T=OH, O) via Alkali Treatment, Angew. Chem. Int. Ed. 57 (2018) 6115-6119. https://doi.org/10.1002/anie.201800887.

[70] X. Xie, Y. Xue, L. Li, S. Chen, Y. Nie, W. Ding, Z. Wei, Surface Al leached Ti_3AlC_2 as a substitute for carbon for use as a catalyst support in a harsh corrosive electrochemical system, Nanoscale 6 (2014) 11035-11040. https://doi.org/10.1039/c4nr02080d.

[71] F. Han, S. Luo, L. Xie, J. Zhu, W. Wei, X. Chen, F. Liu, W. Chen, J. Zhao, L. Dong, K. Yu, X. Zeng, F. Rao, L. Wang, Y. Huang, Boosting the Yield of MXene 2D Sheets via a Facile Hydrothermal-Assisted Intercalation, ACS Appl. Mater. Interfaces 11 (2019) 8443-8452. https://doi.org/10.1021/acsami.8b22339.

[72] S.-Y. Pang, W.-F. Io, L.-W. Wong, J. Zhao, J. Hao, Efficient Energy Conversion and Storage Based on Robust Fluoride-Free Self-Assembled 1D Niobium Carbide in 3D Nanowire Network, Adv. Sci. 7 (2020) 1903680. https://doi.org/10.1002/advs.201903680.

[73] W. Sun, S.A. Shah, Y. Chen, Z. Tan, H. Gao, T. Habib, M. Radovic, M.J. Green, Electrochemical etching of Ti_2AlC to Ti_2CT_x (MXene) in low-concentration hydrochloric acid solution, J. Mater. Chem. A 5 (2017) 21663-21668. https://doi.org/10.1039/c7ta05574a.

[74] S.-Y. Pang, Y.-T. Wong, S. Yuan, Y. Liu, M.-K. Tsang, Z. Yang, H. Huang, W.-T. Wong, J. Hao, Universal Strategy for HF-Free Facile and Rapid Synthesis of Twodimensional MXenes as Multifunctional Energy Materials, J. Am. Chem. Soc. 141 (2019) 9610-9616. https://doi.org/10.1021/jacs.9b02578.

[75] M. Li, J. Lu, K. Luo, Y. Li, K. Chang, K. Chen, J. Zhou, J. Rosen, L. Hultman, P. Eklund, P.O.A. Persson, S. Du, Z. Chai, Z. Huang, Q. Huang, Element Replacement Approach by Reaction with Lewis Acidic Molten Salts to Synthesize Nanolaminated MAX Phases and MXenes, J. Am. Chem. Soc. 141 (2019) 4730-4737. https://doi.org/10.1021/jacs.9b00574.

[76] Y. Li, H. Shao, Z. Lin, J. Lu, L. Liu, B. Duployer, P.O.Å. Persson, P. Eklund, L. Hultman, M. Li, K. Chen, X.-H. Zha, S. Du, P. Rozier, Z. Chai, E. Raymundo-Piñero, P.-L. Taberna, P. Simon, Q. Huang, A general Lewis acidic etching route for preparing MXenes with enhanced electrochemical performance in non-aqueous electrolyte, Nat. Mater. 19 (2020) 894-899. https://doi.org/10.1038/s41563-020-0657-0.

[77] Y. Gogotsi, Chemical vapour deposition: Transition metal carbides go 2D, Nat. Mater. 14 (2015) 1079-1080. https://doi.org/10.1038/nmat4386.

[78] C. Xu, L. Wang, Z. Liu, L. Chen, J. Guo, N. Kang, X.L. Ma, H.M. Cheng, W. Ren, Large-area high-quality 2D ultrathin Mo_2C superconducting crystals, Nat. Mater. 14 (2015) 1135-1141. https://doi.org/10.1038/nmat4374.

[79] D. Geng, X. Zhao, Z. Chen, W. Sun, W. Fu, J. Chen, W. Liu, W. Zhou, K.P. Loh, Direct Synthesis of Large-Area 2D Mo_2C on In Situ Grown Graphene, Adv. Mater. 29 (2017) 1700072. https://doi.org/10.1002/adma.201700072.

[80] X.X. Zhan, C. Si, J. Zhou, Z.M. Sun, MXene and MXene-based composites: synthesis, properties and environment-related applications, Nanoscale Horiz. 5 (2020) 235-258. https://doi.org/10.1039/c9nh00571d.

[81] A. VahidMohammadi, J. Rosen, Y. Gogotsi, The world of two-dimensional carbides and nitrides (MXenes), Science 372 (2021) eabf1581. https://doi.org/10.1126/science.abf1581.

[82] L. Verger, C. Xu, V. Natu, H.-M. Cheng, W. Ren, M.W. Barsoum, Overview of the synthesis of MXenes and other ultrathin 2D transition metal carbides and nitrides, Curr. Opin. Solid State Mater. Sci. 23 (2019) 149-163. https://doi.org/10.1016/j.cossms.2019.02.001.

[83] A.P. Martin Dahlqvist, Jun Lu, Lars Hultman, and Johanna Rosen, Origin of Chemically Ordered Atomic Laminates (i‑MAX): Expanding the Elemental Space by a Theoretical/Experimental Approach, ACS Nano 12 (2018) 7761-7770. https://doi.org/10.1021/acsnano.8b01774.

[84] B. Anasori, C. Shi, E.J. Moon, Y. Xie, C.A. Voigt, P.R.C. Kent, S.J. May, S.J.L. Billinge, M.W. Barsoum, Y. Gogotsi, Control of electronic properties of 2D carbides (MXenes) by manipulating their transition metal layers, Nanoscale Horiz. 1 (2016) 227-234. https://doi.org/10.1039/c5nh00125k.

[85] B. Ahmed, A.E. Ghazaly, J. Rosen, i-MXenes for Energy Storage and Catalysis, Adv. Funct. Mater. 30 (2020) 2000894. https://doi.org/10.1002/adfm.202000894.

[86] A. Iqbal, F. Shahzad, K. Hantanasirisakul, M.-K. Kim, J. Kwon, J. Hong, H. Kim, D. Kim, Y. Gogotsi, C.M. Koo, Anomalous absorption of electromagnetic waves by 2D transition metal carbonitride Ti_3CNT_x (MXene), Science 369 (2020) 446-450. https://doi.org/10.1126/science.aba7977.

[87] N.R. Hemanth, B. Kandasubramanian, Recent advances in 2D MXenes for enhanced cation intercalation in energy harvesting Applications: A review, Chem. Eng. J. 392 (2020) 123678. https://doi.org/10.1016/j.cej.2019.123678.

[88] M. Malaki, A. Maleki, R.S. Varma, MXenes and ultrasonication, J. Mater. Chem. A 7 (2019) 10843-10857. https://doi.org/10.1039/C9TA01850F.

[89] M.R. Lukatskaya, O. Mashtalir, C.E. Ren, Y. Dall'Agnese, P. Rozier, P.L. Taberna, M. Naguib, P. Simon, M.W. Barsoum, Y. Gogotsi, Cation Intercalation and High Volumetric Capacitance of Two-Dimensional Titanium Carbide, Science 341 (2013) 1502-1505. https://doi.org/10.1126/science.1241488.

[90] M. Naguib, R.R. Unocic, B.L. Armstrong, J. Nanda, Large-scale delamination of multi-layers transition metal carbides and carbonitrides "MXenes", Dalton Trans. 44 (2015) 9353-9358. https://doi.org/10.1039/C5DT01247C.

[91] O. Mashtalir, M. Naguib, V.N. Mochalin, Y. Dall'Agnese, M. Heon, M.W. Barsoum, Y. Gogotsi, Intercalation and delamination of layered carbides and carbonitrides, Nat. Commun. 4 (2013) 1716. https://doi.org/10.1038/ncomms2664.

[92] Y. Jiang, T. Sun, X. Xie, W. Jiang, J. Li, B. Tian, C. Su, Oxygen-Functionalized Ultrathin $Ti_3C_2T_x$ MXene for Enhanced Electrocatalytic Hydrogen Evolution, ChemSusChem 12 (2019) 1368-1373. https://doi.org/10.1002/cssc.201803032.

[93] R.Y. Fang, C.W. Lu, A.Q. Chen, K. Wang, H. Huang, Y.P. Gan, C. Liang, J. Zhang, X.Y. Tao, Y. Xia, W.K. Zhang, 2D MXene-based Energy Storage Materials: Interfacial Structure Design and Functionalization, ChemSusChem 13 (2020) 1409-1419. https://doi.org/10.1002/cssc.201902537.

[94] X.H. Zha, K. Luo, Q.W. Li, Q. Huang, J. He, X.D. Wen, S.Y. Du, Role of the surface effect on the structural, electronic and mechanical properties of the carbide MXenes, Epl 111 (2015) 26007. https://doi.org/10.1209/0295-5075/111/26007.

[95] J.L. Hart, K. Hantanasirisakul, A.C. Lang, B. Anasori, D. Pinto, Y. Pivak, J.T. van Omme, S.J. May, Y. Gogotsi, M.L. Taheri, Control of MXenes' electronic properties through termination and intercalation, Nat. commun. 10 (2019) 522. https://doi.org/10.1038/s41467-018-08169-8.

[96] R. Meshkian, M. Dahlqvist, J. Lu, B. Wickman, J. Halim, J. Thornberg, Q. Tao, S. Li, S. Intikhab, J. Snyder, M.W. Barsoum, M. Yildizhan, J. Palisaitis, L. Hultman, P.O.A. Persson, J. Rosen, W-Based Atomic Laminates and Their 2D Derivative $W_{1.33}C$ MXene with Vacancy Ordering, Adv. Mater. 30 (2018) 1706409. https://doi.org/10.1002/adma.201706409.

[97] V. Kamysbayev, A.S. Filatov, H. Hu, X. Rui, F. Lagunas, D. Wang, R.F. Klie, D.V. Talapin, Covalent surface modifications and superconductivity of two-dimensional metal carbide MXenes, Science 369 (2020) 979-983. https://doi.org/10.1126/science.aba8311.

[98] L.H. Karlsson, J. Birch, J. Halim, M.W. Barsoum, P.O. Persson, Atomically Resolved Structural and Chemical Investigation of Single MXene Sheets, Nano lett. 15 (2015) 4955-4960. https://doi.org/10.1021/acs.nanolett.5b00737.

[99] W. Peng, M. Luo, X. Xu, K. Jiang, M. Peng, D. Chen, T.S. Chan, Y. Tan, Spontaneous Atomic Ruthenium Doping in Mo_2CT_x MXene Defects Enhances Electrocatalytic Activity for the Nitrogen Reduction Reaction, Adv. Energy Mater. 10 (2020) 2001364. https://doi.org/10.1002/aenm.202001364.

[100] D. Zhao, Z. Chen, W. Yang, S. Liu, X. Zhang, Y. Yu, W.C. Cheong, L. Zheng, F. Ren, G. Ying, X. Cao, D. Wang, Q. Peng, G. Wang, C. Chen, MXene (Ti_3C_2) Vacancy-Confined Single-Atom Catalyst for Efficient Functionalization of CO_2, J. Am. Chem. Soc. 141 (2019) 4086-4093. https://doi.org/10.1021/jacs.8b13579.

[101] Q. Tao, M. Dahlqvist, J. Lu, S. Kota, R. Meshkian, J. Halim, J. Palisaitis, L. Hultman, M.W. Barsoum, P.O.A. Persson, J. Rosen, Two-dimensional $Mo_{1.33}C$ MXene with divacancy ordering prepared from parent 3D laminate with in-plane chemical ordering, Nat. Commun. 8 (2017) 14949. https://doi.org/10.1038/ncomms14949.

[102] Y. Yan, B.Y. Xia, B. Zhao, X. Wang, A review on noble-metal-free bifunctional heterogeneous catalysts for overall electrochemical water splitting, J. Mater. Chem. A 4 (2016) 17587-17603. https://doi.org/10.1039/C6TA08075H.

[103] Q. Gao, W. Zhang, Z. Shi, L. Yang, Y. Tang, Structural Design and Electronic Modulation of Transition-Metal-Carbide Electrocatalysts toward Efficient Hydrogen Evolution, Adv. Mater. 31 (2019) 1802880. https://doi.org/10.1002/adma.201802880.

[104] Y. Li, J. Wang, X. Tian, L. Ma, C. Dai, C. Yang, Z. Zhou, Carbon doped molybdenum disulfide nanosheets stabilized on graphene for the hydrogen evolution reaction with high electrocatalytic ability, Nanoscale 8 (2016) 1676-1683. https://doi.org/10.1039/C5NR07370G.

[105] C. Hu, L. Zhang, J. Gong, Recent progress made in the mechanism comprehension and design of electrocatalysts for alkaline water splitting, Energy Environ. Sci. 12 (2019) 2620-2645. https://doi.org/10.1039/C9EE01202H.

[106] Y.-W. Cheng, J.-H. Dai, Y.-M. Zhang, Y. Song, Two-Dimensional, Ordered, Double Transition Metal Carbides (MXenes): A New Family of Promising Catalysts for the Hydrogen Evolution Reaction, J. Phys. Chem. C 122 (2018) 28113-28122. https://doi.org/10.1021/acs.jpcc.8b08914.

[107] J. Liang, C. Ding, J. Liu, T. Chen, W. Peng, Y. Li, F. Zhang, X. Fan, Heterostructure engineering of Co-doped MoS_2 coupled with Mo_2CT_x MXene for enhanced hydrogen evolution in alkaline media, Nanoscale 11 (2019) 10992-11000. https://doi.org/10.1039/c9nr02085c.

[108] J. Chen, G. Liu, Y.Z. Zhu, M. Su, P. Yin, X.J. Wu, Q. Lu, C. Tan, M. Zhao, Z. Liu, W. Yang, H. Li, G.H. Nam, L. Zhang, Z. Chen, X. Huang, P.M. Radjenovic, W. Huang, Z.Q. Tian, J.F. Li, H. Zhang, Ag@MoS_2 Core-Shell Heterostructure as SERS Platform to Reveal the Hydrogen Evolution Active Sites of Single-Layer MoS_2, J. Am. Chem. Soc. 142 (2020) 7161-7167. https://doi.org/10.1021/jacs.0c01649.

[109] S. Li, P. Tuo, J. Xie, X. Zhang, J. Xu, J. Bao, B. Pan, Y. Xie, Ultrathin MXene nanosheets with rich fluorine termination groups realizing efficient electrocatalytic hydrogen evolution, Nano Energy 47 (2018) 512-518. https://doi.org/10.1016/j.nanoen.2018.03.022.

[110] H. Pan, Ultra-high electrochemical catalytic activity of MXenes, Sci. Rep. 6 (2016) 32531. https://doi.org/10.1038/srep32531.

[111] C. Ling, L. Shi, Y. Ouyang, J. Wang, Searching for Highly Active Catalysts for Hydrogen Evolution Reaction Based on O^- Terminated MXenes through a Simple Descriptor, Chem. Mater. 28 (2016) 9026-9032. https://doi.org/10.1021/acs.chemmater.6b03972.

[112] D. Merki, H. Vrubel, L. Rovelli, S.e. Fierro, X. Hu, Fe, Co, and Ni ions promote the catalytic activity of amorphous molybdenum sulfide films for hydrogen evolution, Chem. Sci. 3 (2012) 2515. https://doi.org/10.1039/c2sc20539d.

[113] C. Tsai, K. Chan, J.K. Nørskovab, F. Abild-Pedersen, Rational design of MoS_2 catalysts: tuning the structure and activity via transition metal doping, Catal. Sci. Technol. 5 (2015) 246. https://doi.org/10.1039/c4cy01162g.

[114] S. Wang, L. Chen, Y. Wu, Q. Zhang, Surface Modifications of Ti_2CO_2 for Obtaining High Hydrogen Evolution Reaction Activity and Conductivity: A Computational Approach, Chemphyschem 19 (2018) 3380-3387. https://doi.org/10.1002/cphc.201800899.

[115] X. Sun, J. Zheng, Y. Gao, C. Qiu, Y. Yan, Z. Yao, S. Deng, J. Wang, Machine-learning-accelerated screening of hydrogen evolution catalysts in MBenes materials, Appl. Surf. Sci. 526 (2020) 146522. https://doi.org/10.1016/j.apsusc.2020.146522.

[116] M. Wang, H. Zhu, Machine Learning for Transition-Metal-Based Hydrogen Generation Electrocatalysts, ACS Catal. 11 (2021) 3930-3937. https://doi.org/10.1021/acscatal.1c00178.

[117] X. Wang, Y. Su, M. Song, K. Song, M. Chen, P. Qian, Design single nonmetal atom doped 2D Ti_2CO_2 electrocatalyst for hydrogen evolution reaction by coupling electronic descriptor, Appl. Surf. Sci. 556 (2021) 149778. https://doi.org/10.1016/j.apsusc.2021.149778.

[118] J. Zheng, X. Sun, C. Qiu, Y. Yan, Z. Yao, S. Deng, X. Zhong, G. Zhuang, Z. Wei, J. Wang, High-Throughput Screening of Hydrogen Evolution Reaction Catalysts in MXene Materials, J. Phys. Chem. C 124 (2020) 13695-13705. https://doi.org/10.1021/acs.jpcc.0c02265.

[119] T.L. Tan, H.M. Jin, M.B. Sullivan, B. Anasori, Y. Gogotsi, High-Throughput Survey of Ordering Configurations in MXene Alloys Across Compositions and Temperatures, ACS Nano 11 (2017) 4407-4418. https://doi.org/10.1021/acsnano.6b08227.

[120] X. Wang, C. Wang, S. Ci, Y. Ma, T. Liu, L. Gao, P. Qian, C. Ji, Y. Su, Accelerating 2D MXene catalyst discovery for the hydrogen evolution reaction by computer-driven workflow and an ensemble learning strategy, Journal of Materials Chemistry A 8 (2020) 23488-23497. https://doi.org/10.1039/d0ta06583h.

[121] M. Pandey, K.S. Thygesen, Two-Dimensional MXenes as Catalysts for Electrochemical Hydrogen Evolution: A Computational Screening Study, J. Phys. Chem. C 121 (2017) 13593-13598. https://doi.org/10.1021/acs.jpcc.7b05270.

[122] Y.-W. Cheng, J.-H. Dai, Y.-M. Zhang, Y. Song, Transition metal modification and carbon vacancy promoted Cr_2CO_2(MXenes): a new opportunity for a highly active catalyst for the hydrogen evolution reaction, J. Mater. Chem. A 6 (2018) 20956-20965. https://doi.org/10.1039/c8ta07749e.

[123] S. Intikhab, V. Natu, J. Li, Y. Li, Q. Tao, J. Rosen, M.W. Barsoum, J. Snyder, Stoichiometry and surface structure dependence of hydrogen evolution reaction activity and stability of Mo_xC MXenes, J. Catal. 371 (2019) 325-332. https://doi.org/10.1016/j.jcat.2019.01.037.

[124] Y. Ito, W. Cong, T. Fujita, Z. Tang, M. Chen, High catalytic activity of nitrogen and sulfur co-doped nanoporous graphene in the hydrogen evolution reaction, Angew. Chem. Int. Ed. 54 (2015) 2131-2136. https://doi.org/10.1002/anie.201410050.

[125] T.A. Le, Q.V. Bui, N.Q. Tran, Y. Cho, Y. Hong, Y. Kawazoe, H. Lee, Synergistic Effects of Nitrogen Doping on MXene for Enhancement of Hydrogen Evolution Reaction, ACS Sustain. Chem. Eng. 7 (2019) 16879-16888. https://doi.org/10.1021/acssuschemeng.9b04470.

[126] Y. Yoon, A.P. Tiwari, M. Choi, T.G. Novak, W. Song, H. Chang, T. Zyung, S.S. Lee, S. Jeon, K.-S. An, Precious-Metal-Free Electrocatalysts for Activation of Hydrogen Evolution with Nonmetallic Electron Donor: Chemical Composition Controllable Phosphorous Doped Vanadium Carbide MXene, Adv. Funct. Mater. 29 (2019) 1903443. https://doi.org/10.1002/adfm.201903443.

[127] C. Ling, L. Shi, Y. Ouyang, Q. Chen, J. Wang, Transition Metal-Promoted V_2CO_2 (MXenes): A New and Highly Active Catalyst for Hydrogen Evolution Reaction, Adv. Sci. 3 (2016) 1600180. https://doi.org/10.1002/advs.201600180.

[128] P. Li, J. Zhu, A.D. Handoko, R. Zhang, H. Wang, D. Legut, X. Wen, Z. Fu, Z.W. Seh, Q. Zhang, High-throughput theoretical optimization of the hydrogen evolution reaction on MXenes by transition metal modification, J. Mater. Chem. A 6 (2018) 4271-4278. https://doi.org/10.1039/c8ta00173a.

[129] D.A. Kuznetsov, Z. Chen, P.V. Kumar, A. Tsoukalou, A. Kierzkowska, P.M. Abdala, O.V. Safonova, A. Fedorov, C.R. Muller, Single Site Cobalt Substitution in 2D Molybdenum Carbide (MXene) Enhances Catalytic Activity in the Hydrogen Evolution Reaction, J. Am. Chem. Soc. 141 (2019) 17809-17816. https://doi.org/10.1021/jacs.9b08897.

[130] Z. Li, Z. Qi, S. Wang, T. Ma, L. Zhou, Z. Wu, X. Luan, F.Y. Lin, M. Chen, J.T. Miller, H. Xin, W. Huang, Y. Wu, In Situ Formed Pt_3Ti Nanoparticles on a Two-Dimensional Transition Metal Carbide (MXene) Used as Efficient Catalysts for Hydrogen Evolution Reactions, Nano Lett. 19 (2019) 5102-5108. https://doi.org/10.1021/acs.nanolett.9b01381.

[131] X. Wu, S. Zhou, Z. Wang, J. Liu, W. Pei, P. Yang, J. Zhao, J. Qiu, Engineering Multifunctional Collaborative Catalytic Interface Enabling Efficient Hydrogen Evolution in All pH Range and Seawater, Adv. Energy Mater. 9 (2019) 1901333. https://doi.org/10.1002/aenm.201901333.

[132] Y. Jiang, X. Wu, Y. Yan, S. Luo, X. Li, J. Huang, H. Zhang, D. Yang, Coupling PtNi Ultrathin Nanowires with MXenes for Boosting Electrocatalytic Hydrogen Evolution in Both Acidic and Alkaline Solutions, Small 15 (2019) 1805474. https://doi.org/10.1002/smll.201805474.

[133] C.-F. Du, X. Sun, H. Yu, Q. Liang, K.N. Dinh, Y. Zheng, Y. Luo, Z. Wang, Q. Yan, Synergy of Nb Doping and Surface Alloy Enhanced on Water-Alkali Electrocatalytic Hydrogen Generation Performance in Ti-Based MXene, Adv. Sci. 6 (2019) 1900116. https://doi.org/10.1002/advs.201900116.

[134] Y. Yuan, H. Li, L. Wang, L. Zhang, D. Shi, Y. Hong, J. Sun, Achieving Highly Efficient Catalysts for Hydrogen Evolution Reaction by Electronic State Modification of Platinum on Versatile $Ti_3C_2T_x$ (MXene), ACS Sustain. Chem. Eng. 7 (2019) 4266-4273. https://doi.org/10.1021/acssuschemeng.8b06045.

[135] X. Wu, Z. Wang, M. Yu, L. Xiu, J. Qiu, Stabilizing the MXenes by Carbon Nanoplating for Developing Hierarchical Nanohybrids with Efficient Lithium Storage and Hydrogen Evolution Capability, Adv. Mater. 29 (2017) 1607017. https://doi.org/10.1002/adma.201607017.

[136] H. Jiang, Z. Wang, Q. Yang, L. Tan, L. Dong, M. Dong, Ultrathin $Ti_3C_2T_x$ (MXene) Nanosheet-Wrapped $NiSe_2$ Octahedral Crystal for Enhanced Supercapacitor Performance and Synergetic Electrocatalytic Water Splitting, Nano-Micro Lett. 11 (2019) 31. https://doi.org/10.1007/s40820-019-0261-5.

[137] M. Yu, Z. Wang, J. Liu, F. Sun, P. Yang, J. Qiu, A hierarchically porous and hydrophilic 3D nickel-iron/MXene electrode for accelerating oxygen and hydrogen evolution at high current densities, Nano Energy 63 (2019) 103880. https://doi.org/10.1016/j.nanoen.2019.103880.

[138] V. Ramalingam, P. Varadhan, H.-C. Fu, H. Kim, D. Zhang, S. Chen, L. Song, D. Ma, Y. Wang, H.N. Alshareef, J.-H. He, Heteroatom-Mediated Interactions between Ruthenium Single Atoms and an MXene Support for Efficient Hydrogen Evolution, Adv. Mater. 31 (2019) 1903841. https://doi.org/10.1002/adma.201903841.

[139] H. Liu, Z. Hu, Q. Liu, P. Sun, Y. Wang, S. Chou, Z. Hu, Z. Zhang, Single-atom Ru anchored in nitrogen-doped MXene ($Ti_3C_2T_x$) as an efficient catalyst for the hydrogen evolution reaction at all pH values, J. Mater. Chem. A 8 (2020) 24710-24717. https://doi.org/10.1039/d0ta09538a.

[140] Z. Wang, W. Xu, K. Yu, Y. Feng, Z. Zhu, 2D heterogeneous vanadium compound interfacial modulation enhanced synergistic catalytic hydrogen evolution for full pH range seawater splitting, Nanoscale 12 (2020) 6176-6187. https://doi.org/10.1039/D0NR00207K.

[141] J. Liu, Y. Liu, D. Xu, Y. Zhu, W. Peng, Y. Li, F. Zhang, X. Fan, Hierarchical “nanoroll” like $MoS_2/Ti_3C_2T_x$ hybrid with high electrocatalytic hydrogen evolution activity, Appl. Catal. B Environ. 241 (2019) 89-94. https://doi.org/10.1016/j.apcatb.2018.08.083.

[142] J. Ren, H. Zong, Y. Sun, S. Gong, Y. Feng, Z. Wang, L. Hu, K. Yu, Z. Zhu, 2D organ-like molybdenum carbide (MXene) coupled with MoS_2 nanoflowers enhances the catalytic activity in the hydrogen evolution reaction, CrystEngComm 22 (2020) 1395-1403. https://doi.org/10.1039/C9CE01777A.

[143] S. Han, Y. Chen, Y. Hao, Y. Xie, D. Xie, Y. Chen, Y. Xiong, Z. He, F. Hu, L. Li, J. Zhu, S. Peng, Multi-dimensional hierarchical CoS_2@MXene as trifunctional electrocatalysts for zinc-air batteries and overall water splitting, Sci. China Mater. 64 (2020) 1127-1138. https://doi.org/10.1007/s40843-020-1524-5.

[144] L. Yan, B. Zhang, S. Wu, J. Yu, A general approach to the synthesis of transition metal phosphide nanoarrays on MXene nanosheets for pH-universal hydrogen evolution and alkaline overall water splitting, J. Mater. Chem. A 8 (2020) 14234-14242. https://doi.org/10.1039/d0ta05189f.

[145] J. Filip, S. Zavahir, L. Lorencova, T. Bertok, A.B. Yousaf, K.A. Mahmoud, J. Tkac, P. Kasak, Tailoring Electrocatalytic Properties of Pt Nanoparticles Grown on $Ti_3C_2T_x$ MXene Surface, J. Electrochem. Soc. 166 (2019) H54-H62. https://doi.org/10.1149/2.0991902jes.

[146] X. Li, X. Lv, X. Sun, C. Yang, Y.-Z. Zheng, L. Yang, S. Li, X. Tao, Edge-oriented, high-percentage 1T'-phase MoS_2 nanosheets stabilize Ti_3C_2 MXene for efficient electrocatalytic hydrogen evolution, Appl. Catal. B Environ. 284 (2021) 119708. https://doi.org/10.1016/j.apcatb.2020.119708.

[147] W. Xiao, D. Yan, Y. Zhang, X. Yang, T. Zhang, Heterostructured $MoSe_2$/Oxygen-Terminated Ti_3C_2 MXene Architectures for Efficient Electrocatalytic Hydrogen Evolution, Energy Fuels 35 (2021) 4609-4615. https://doi.org/10.1021/acs.energyfuels.1c00123.

[148] S. Zhang, H. Zhuo, S. Li, Z. Bao, S. Deng, G. Zhuang, X. Zhong, Z. Wei, Z. Yao, J.-g. Wang, Effects of surface functionalization of mxene-based nanocatalysts on hydrogen evolution reaction performance, Catal. Today 368 (2020) 187-195. https://doi.org/10.1016/j.cattod.2020.02.002.

[149] C. Cui, R. Cheng, H. Zhang, C. Zhang, Y. Ma, C. Shi, B. Fan, H. Wang, X. Wang, Ultrastable MXene@Pt/SWCNTs' Nanocatalysts for Hydrogen Evolution Reaction, Adv. Funct. Mater. 30 (2020) 2000693. https://doi.org/10.1002/adfm.202000693.

[150] S. Li, X. Que, X. Chen, T. Lin, L. Sheng, J. Peng, J. Li, M. Zhai, One-Step Synthesis of Modified Ti_3C_2 MXene-Supported Amorphous Molybdenum Sulfide Electrocatalysts by a Facile Gamma Radiation Strategy for Efficient Hydrogen Evolution Reaction, ACS Appl. Energy Mater. 3 (2020) 10882-10891. https://doi.org/10.1021/acsaem.0c01900.

[151] N.T. Suen, S.F. Hung, Q. Quan, N. Zhang, Y.J. Xu, H.M. Chen, Electrocatalysis for the oxygen evolution reaction: recent development and future perspectives, Chem. Soc. Rev. 46 (2017) 337-365. https://doi.org/10.1039/c6cs00328a.

[152] F. Song, L. Bai, A. Moysiadou, S. Lee, C. Hu, L. Liardet, X. Hu, Transition Metal Oxides as Electrocatalysts for the Oxygen Evolution Reaction in Alkaline Solutions: An Application-Inspired Renaissance, J. Am. Chem. Soc. 140 (2018) 7748-7759. https://doi.org/10.1021/jacs.8b04546.

[153] D.A. Kuznetsov, B. Han, Y. Yu, R.R. Rao, J. Hwang, Y. Román-Leshkov, Y. Shao-Horn, Tuning Redox Transitions via Inductive Effect in Metal Oxides and Complexes, and Implications in Oxygen Electrocatalysis, Joule 2 (2018) 225-244. https://doi.org/10.1016/j.joule.2017.11.014.

[154] J. Suntivich, K.J. May, H.A. Gasteiger, J.B. Goodenough, Y. Shao-Horn, A Perovskite Oxide Optimized for Oxygen Evolution Catalysis from Molecular Orbital Principles, Science 334 (2011) 1383. https://doi.org/10.1126/science.1212858.

[155] C. Yang, Y. Tang, Y. Tian, Y. Luo, M. Faraz Ud Din, X. Yin, W. Que, Flexible Nitrogen-Doped 2D Titanium Carbides (MXene) Films Constructed by an Ex Situ Solvothermal Method with

Extraordinary Volumetric Capacitance, Adv. Energy Mater. 8 (2018) 1802087. https://doi.org/10.1002/aenm.201802087.

[156] C. Lu, L. Yang, B. Yan, L. Sun, P. Zhang, W. Zhang, Z. Sun, Nitrogen-Doped Ti_3C_2 MXene: Mechanism Investigation and Electrochemical Analysis, Adv. Funct. Mater. 30 (2020) 2000852. https://doi.org/10.1002/adfm.202000852.

[157] Y. Tang, C. Yang, Y. Tian, Y. Luo, X. Yin, W. Que, The effect of in situ nitrogen doping on the oxygen evolution reaction of MXenes, Nanoscale Adv. 2 (2020) 1187. https://doi.org/10.1039/C9NA00706G.

[158] C. Zhang, B. Ma, Y. Zhou, C. Wang, Highly active and durable Pt/MXene nanocatalysts for ORR in both alkaline and acidic conditions, J. Electroanal. Chem. 865 (2020) 114142. https://doi.org/10.1016/j.jelechem.2020.114142.

[159] Y. Lu, D. Fan, Z. Chen, W. Xiao, C. Cao, X. Yang, Anchoring Co_3O_4 nanoparticles on MXene for efficient electrocatalytic oxygen evolution, Sci. Bull. 65 (2020) 460-466. https://doi.org/10.1016/j.scib.2019.12.020.

[160] K. Zhao, X. Ma, S. Lin, Z. Xu, L. Li, Ambient Growth of Hierarchical FeOOH/MXene as Enhanced Electrocatalyst for Oxygen Evolution Reaction, ChemistrySelect 5 (2020) 1890-1895. https://doi.org/10.1002/slct.201904506.

[161] L. Hu, M. Li, X. Wei, H. Wang, Y. Wu, J. Wen, W. Gu, C. Zhu, Modulating interfacial electronic structure of CoNi LDH nanosheets with $Ti_3C_2T_x$ MXene for enhancing water oxidation catalysis, Chem. Eng. J. 398 (2020) 125605. https://doi.org/10.1016/j.cej.2020.125605.

[162] L. Yao, Q. Gu, X. Yu, Three-Dimensional MOFs@MXene Aerogel Composite Derived MXene Threaded Hollow Carbon Confined CoS Nanoparticles toward Advanced Alkali-Ion Batteries, ACS Nano 15 (2021) 3228-3240. https://doi.org/10.1021/acsnano.0c09898.

[163] L. Zhao, B. Dong, S. Li, L. Zhou, L. Lai, Z. Wang, S. Zhao, M. Han, K. Gao, M. Lu, X. Xie, B. Chen, Z. Liu, X. Wang, H. Zhang, H. Li, J. Liu, H. Zhang, X. Huang, W. Huang, Interdiffusion Reaction-Assisted Hybridization of Two-Dimensional Metal-Organic Frameworks and $Ti_3C_2T_x$ Nanosheets for Electrocatalytic Oxygen Evolution, ACS Nano 11 (2017) 5800-5807. https://doi.org/10.1021/acsnano.7b01409.

[164] M. Benchakar, T. Bilyk, C. Garnero, L. Loupias, C. Morais, J. Pacaud, C. Canaff, P. Chartier, S. Morisset, N. Guignard, V. Mauchamp, S. Célérier, A. Habrioux, MXene Supported Cobalt Layered Double Hydroxide Nanocrystals: Facile Synthesis Route for a Synergistic Oxygen Evolution Reaction Electrocatalyst, Adv. Mater. Interfaces 6 (2019) 1901328. https://doi.org/10.1002/admi.201901328.

[165] J. Liu, T. Chen, P. Juan, W. Peng, Y. Li, F. Zhang, X. Fan, Hierarchical Cobalt Borate/MXenes Hybrid with Extraordinary Electrocatalytic Performance in Oxygen Evolution Reaction, ChemSusChem 11 (2018) 3758-3765. https://doi.org/10.1002/cssc.201802098.

[166] C. Hao, Y. Wu, Y. An, B. Cui, J. Lin, X. Li, D. Wang, M. Jiang, Z. Cheng, S. Hu, Interface-coupling of CoFe-LDH on MXene as high-performance oxygen evolution catalyst, Mater. Today Energy 12 (2019) 453-462. https://doi.org/10.1016/j.mtener.2019.04.009.

[167] J. Chen, Q. Long, K. Xiao, T. Ouyang, N. Li, S. Ye, Z.-Q. Liu, Vertically-interlaced NiFeP/MXene electrocatalyst with tunable electronic structure for high-efficiency oxygen evolution reaction, Sci. Bull. 66 (2021) 1063-1072. https://doi.org/10.1016/j.scib.2021.02.033.

[168] N. Hao, Y. Wei, J. Wang, Z. Wang, Z. Zhu, S. Zhao, M. Han, X. Huang, In situ hybridization of an MXene/TiO_2/NiFeCo-layered double hydroxide composite for electrochemical and photoelectrochemical oxygen evolution, RSC Adv. 8 (2018) 20576-20584. https://doi.org/10.1039/C8RA02349B.

[169] Y. Tang, C. Yang, Y. Yang, X. Yin, W. Que, J. Zhu, Three dimensional hierarchical network structure of S-$NiFe_2O_4$ modified few-layer titanium carbides (MXene) flakes on nickel foam as a high efficient electrocatalyst for oxygen evolution, Electrochim. Acta 296 (2019) 762-770. https://doi.org/10.1016/j.electacta.2018.11.083.

[170] N. Li, Y. Zhang, M. Jia, X. Lv, X. Li, R. Li, X. Ding, Y.-Z. Zheng, X. Tao, 1T/2H $MoSe_2$-on-MXene heterostructure as bifunctional electrocatalyst for efficient overall water splitting, Electrochim. Acta 326 (2019) 134976. https://doi.org/10.1016/j.electacta.2019.134976.

[171] Y. Zhang, H. Jiang, Y. Lin, H. Liu, Q. He, C. Wu, T. Duan, L. Song, In Situ Growth of Cobalt Nanoparticles Encapsulated Nitrogen-Doped Carbon Nanotubes among $Ti_3C_2T_x$ (MXene) Matrix for Oxygen Reduction and Evolution, Adv. Mater. Interfaces 5 (2018) 1800392. https://doi.org/10.1002/admi.201800392.

[172] H. Zou, B. He, P. Kuang, J. Yu, K. Fan, Metal-Organic Framework-Derived Nickel-Cobalt Sulfide on Ultrathin Mxene Nanosheets for Electrocatalytic Oxygen Evolution, ACS Appl. Mater. Interfaces 10 (2018) 22311-22319. https://doi.org/10.1021/acsami.8b06272.

[173] L. Xiu, Z. Wang, M. Yu, X. Wu, J. Qiu, Aggregation-Resistant 3D MXene-Based Architecture as Efficient Bifunctional Electrocatalyst for Overall Water Splitting, ACS Nano 12 (2018) 8017-8028. https://doi.org/10.1021/acsnano.8b02849.

[174] C. Wang, X.-D. Zhu, Y.-C. Mao, F. Wang, X.-T. Gao, S.-Y. Qiu, S.-R. Le, K.-N. Sun, MXene-supported Co_3O_4 quantum dots for superior lithium storage and oxygen evolution activities, Chem. Commun. 55 (2019) 1237-1240. https://doi.org/10.1039/C8CC09699F.

[175] Z. Wu, H. Wang, P. Xiong, G. Li, T. Qiu, W.B. Gong, F. Zhao, C. Li, Q. Li, G. Wang, F. Geng, Molecularly Thin Nitride Sheets Stabilized by Titanium Carbide as Efficient Bifunctional

Electrocatalysts for Fiber-Shaped Rechargeable Zinc-Air Batteries, Nano lett. 20 (2020) 2892-2898. https://doi.org/10.1021/acs.nanolett.0c00717.

[176] B. Cui, B. Hu, J. Liu, M. Wang, Y. Song, K. Tian, Z. Zhang, L. He, Solution-Plasma-Assisted Bimetallic Oxide Alloy Nanoparticles of Pt and Pd Embedded within Two-Dimensional $Ti_3C_2T_x$ Nanosheets as Highly Active Electrocatalysts for Overall Water Splitting, ACS Appl. Mater. Interfaces 10 (2018) 23858-23873. https://doi.org/10.1021/acsami.8b06568.

[177] Q. Yue, J. Sun, S. Chen, Y. Zhou, H. Li, Y. Chen, R. Zhang, G. Wei, Y. Kang, Hierarchical Mesoporous MXene-NiCoP Electrocatalyst for Water-Splitting, ACS Appl. Mater. Interfaces 12 (2020) 18570-18577. https://doi.org/10.1021/acsami.0c01303.

[178] L. Yan, X. Chen, X. Liu, L. Chen, B. Zhang, In situ formed VOOH nanosheet arrays anchored on a $Ti_3C_2T_x$ MXene as a highly efficient and robust synergistic electrocatalyst for boosting water oxidation and reduction, J. Mater. Chem. A 8 (2020) 23637-23644. https://doi.org/10.1039/d0ta09410b.

[179] X. Wen, Q. Zhang, J. Guan, Applications of metal-organic framework-derived materials in fuel cells and metal-air batteries, Coord. Chem. Rev. 409 (2020) 213214. https://doi.org/10.1016/j.ccr.2020.213214.

[180] Z.-F. Huang, J. Wang, Y. Peng, C.-Y. Jung, A. Fisher, X. Wang, Design of Efficient Bifunctional Oxygen Reduction/Evolution Electrocatalyst: Recent Advances and Perspectives, Adv. Energy Mater. 7 (2017) 1700544. https://doi.org/10.1002/aenm.201700544.

[181] Z. Liang, N. Kong, C. Yang, W. Zhang, H. Zheng, H. Lin, R. Cao, Highly Curved Nanostructures Coated Co, N-Doped Carbon Materials for Oxygen Electrocatalysis, Angew. Chem. Int. Ed. 133 (2021) 12859-12874. https://doi.org/10.1002/anie.202101562.

[182] H.W. Kim, V.J. Bukas, H. Park, S. Park, K.M. Diederichsen, J. Lim, Y.H. Cho, J. Kim, W. Kim, T.H. Han, J. Voss, A.C. Luntz, B.D. McCloskey, Mechanisms of Two-Electron and Four-Electron Electrochemical Oxygen Reduction Reactions at Nitrogen-Doped Reduced Graphene Oxide, ACS Catal. 10 (2020) 852-863. https://doi.org/10.1021/acscatal.9b04106.

[183] A. Kulkarni, S. Siahrostami, A. Patel, J.K. Nørskov, Understanding Catalytic Activity Trends in the Oxygen Reduction Reaction, Chem. Rev. 118 (2018) 2302-2312. https://doi.org/10.1021/acs.chemrev.7b00488.

[184] J. Suntivich, H.A. Gasteiger, N. Yabuuchi, H. Nakanishi, J.B. Goodenough, Y. Shao-Horn, Design principles for oxygen-reduction activity on perovskite oxide catalysts for fuel cells and metal-air batteries, Nat. Chem. 3 (2011) 546-550. https://doi.org/10.1038/nchem.1069.

[185] C.Y. Liu, E.Y. Li, Termination Effects of Pt/v-$Ti_{n+1}C_nT_2$ MXene Surfaces for Oxygen Reduction Reaction Catalysis, ACS Appl. Mater. Interfaces 11 (2019) 1638-1644. https://doi.org/10.1021/acsami.8b17600.

[186] Q. Peng, J. Zhou, J. Chen, T. Zhang, Z. Sun, Cu single atoms on Ti_2CO_2 as a highly efficient oxygen reduction catalyst in a proton exchange membrane fuel cell, J. Mater. Chem. A 7 (2019) 26062. https://doi.org/10.1039/C9TA08297B.

[187] Z. Zhang, H. Li, G. Zou, C. Fernandez, B. Liu, Q. Zhang, J. Hu, Q. Peng, Self-Reduction Synthesis of New MXene/Ag Composites with Unexpected Electrocatalytic Activity, ACS Sustain. Chem. Eng. 4 (2016) 6763-6771. https://doi.org/10.1021/acssuschemeng.6b01698.

[188] S. Zhou, X. Yang, W. Pei, N. Liu, J. Zhao, Heterostructures of MXenes and N-doped graphene as highly active bifunctional electrocatalysts, Nanoscale 10 (2018) 10876-10883. https://doi.org/10.1039/c8nr01090k.

[189] X. Yu, W. Yin, T. Wang, Y. Zhang, Decorating g-C3N4 Nanosheets with Ti_3C_2 MXene Nanoparticles for Efficient Oxygen Reduction Reaction, Langmuir 35 (2019) 2909-2916. https://doi.org/10.1021/acs.langmuir.8b03456.

[190] Y. Wen, C. Ma, Z. Wei, X. Zhu, Z. Li, FeNC/MXene hybrid nanosheet as an efficient electrocatalyst for oxygen reduction reaction, RSC Adv. 9 (2019) 13424. https://doi.org/10.1039/C9RA01330J.

[191] Z. Li, Z. Zhuang, F. Lv, H. Zhu, L. Zhou, M. Luo, J. Zhu, Z. Lang, S. Feng, W. Chen, L. Mai, S. Guo, The Marriage of the FeN4 Moiety and MXene Boosts Oxygen Reduction Catalysis: Fe 3d Electron Delocalization Matters, Adv. Mater. 30 (2018) 1803220. https://doi.org/10.1002/adma.201803220.

[192] J. Chen, X. Yuan, F. Lyu, Q. Zhong, H. Hu, Q. Pan, Q. Zhang, Integrating MXene nanosheets with cobalt-tipped carbon nanotubes for an efficient oxygen reduction reaction, J. Mater. Chem. A 7 (2019) 1281-1286. https://doi.org/10.1039/c8ta10574j.

[193] W.-T. Wang, N. Batool, T.-H. Zhang, J. Liu, X.-F. Han, J.-H. Tian, R. Yang, When MOFs meet MXenes: superior ORR performance in both alkaline and acidic solutions, J. Mater. Chem. A 9 (2021) 3952-3960. https://doi.org/10.1039/d0ta10811a.

[194] L. Chen, Y. Lin, J. Fu, J. Xie, R. Chen, H. Zhang, Hybridization of Binary Non-Precious-Metal Nanoparticles with d-Ti_3C_2 MXene for Catalyzing the Oxygen Reduction Reaction, ChemElectroChem 5 (2018) 3307-3314. https://doi.org/10.1002/celc.201800693.

[195] Q. Xue, Z. Pei, Y. Huang, M. Zhu, Z. Tang, H. Li, Y. Huang, N. Li, H. Zhang, C. Zhi, Mn_3O_4 nanoparticles on layer-structured Ti_3C_2 MXene towards the oxygen reduction reaction and zinc-air batteries, J. Mater. Chem. A 5 (2017) 20818-20823. https://doi.org/10.1039/c7ta04532h.

[196] Y. Lei, N. Tan, Y. Zhu, D. Huo, S. Sun, Y. Zhang, G. Gao, Synthesis of Porous N-Rich Carbon/MXene from MXene@Polypyrrole Hybrid Nanosheets as Oxygen Reduction Reaction Electrocatalysts, J. Electrochem. Soc. 167 (2020) 116503. https://doi.org/10.1149/1945-7111/aba15b.

[197] X. Yang, Q. Jia, F. Duan, B. Hu, M. Wang, L. He, Y. Song, Z. Zhang, Multiwall carbon nanotubes loaded with MoS_2 quantum dots and MXene quantum dots: Non-Pt bifunctional catalyst for the methanol oxidation and oxygen reduction reactions in alkaline solution, Appl. Surf. Sci. 464 (2019) 78-87. https://doi.org/10.1016/j.apsusc.2018.09.069.

[198] C. Xu, C. Fan, X. Zhang, H. Chen, X. Liu, Z. Fu, R. Wang, T. Hong, J. Cheng, MXene ($Ti_3C_2T_x$) and Carbon Nanotube Hybrid-Supported Platinum Catalysts for the High-Performance Oxygen Reduction Reaction in PEMFC, ACS Appl. Mater. Interfaces 12 (2020) 19539-19546. https://doi.org/10.1021/acsami.0c02446.

[199] H. Parse, I.M. Patil, A.S. Swami, B.A. Kakade, TiO_2-Decorated Titanium Carbide MXene co-Doped with Nitrogen and Sulfur for Oxygen Electroreduction, ACS Appl. Nano Mater. 4 (2021) 1094-1103. https://doi.org/10.1021/acsanm.0c02695.

[200] Z.L. Wang, D. Xu, J.J. Xu, X.B. Zhang, Oxygen electrocatalysts in metal-air batteries: from aqueous to nonaqueous electrolytes, Chem. Soc. Rev. 43 (2014) 7746-7786. https://doi.org/10.1039/c3cs60248f.

[201] H.J. Cui, M.G. Jiao, Y.N. Chen, Y.B. Guo, L.P. Yang, Z.J. Xie, Z. Zhou, S.J. Guo, Molten-Salt-Assisted Synthesis of 3D Holey N-Doped Graphene as Bifunctional Electrocatalysts for Rechargeable Zn-Air Batteries, Small Methods 2 (2018) 1800144. https://doi.org/10.1002/smtd.201800144.

[202] A. Ostadhossein, J. Guo, F. Simeski, M. Ihme, Functionalization of 2D materials for enhancing OER/ORR catalytic activity in Li-oxygen batteries, Commun. Chem. 2 (2019) 95. https://doi.org/10.1038/s42004-019-0196-2.

[203] Z. Wang, X. Chen, F. Shen, X. Hang, C. Niu, TiC MXene High Energy Density Cathode for Lithium-Air Battery, Adv. Theory Simul. 1 (2018) 1800059. https://doi.org/10.1002/adts.201800059.

[204] Y. Yang, M. Yao, X. Wang, H. Huang, Theoretical Prediction of Catalytic Activity of Ti_2C MXene as Cathode for Li-O_2 Batteries, J. Phys. Chem. C 123 (2019) 17466-17471. https://doi.org/10.1021/acs.jpcc.9b05698.

[205] J. Li, K. Han, J. Huang, G. Li, S. Peng, N. Li, J. Wang, W. Zhang, Y. Du, Y. Fan, W. Wang, F. Dang, Polarized nucleation and efficient decomposition of Li_2O_2 for Ti_2C MXene cathode catalyst under a mixed surface condition in lithium-oxygen batteries, Energy Storage Mater. 35 (2021) 669-678. https://doi.org/10.1016/j.ensm.2020.12.004.

[206] G. Li, N. Li, S. Peng, B. He, J. Wang, Y. Du, W. Zhang, K. Han, F. Dang, Highly Efficient Nb_2C MXene Cathode Catalyst with Uniform O-Terminated Surface for Lithium-Oxygen Batteries, Adv. Energy Mater. 11 (2020) 2002721. https://doi.org/10.1002/aenm.202002721.

[207] R. Zheng, C. Shu, Z. Hou, A. Hu, P. Hei, T. Yang, J. Li, R. Liang, J. Long, In Situ Fabricating Oxygen Vacancy-Rich TiO_2 Nanoparticles via Utilizing Thermodynamically Metastable Ti Atoms

on $Ti_3C_2T_x$ MXene Nanosheet Surface To Boost Electrocatalytic Activity for High-Performance Li-O_2 Batteries, ACS Appl. Mater. Interfaces 11 (2019) 46696-46704. https://doi.org/10.1021/acsami.9b14783.

[208] R.X. Zheng, C.Z. Shu, Z.Q. Hou, A.J. Hu, J.X. Zhao, Y.W. Guo, M. He, Y. Yan, J.P. Long, Interfacial electronic structure design of MXene-based electrocatalyst via vacancy modulation for lithium-oxygen battery, Carbon 166 (2020) 273-283. https://doi.org/10.1016/j.carbon.2020.05.059.

[209] Z. Sun, M. Yuan, L. Lin, H. Yang, C. Nan, G. Sun, H. Li, X. Yang, Perovskite $La_{0.5}Sr_{0.5}CoO_{3-\delta}$ Grown on $Ti_3C_2T_x$ MXene Nanosheets as Bifunctional Efficient Hybrid Catalysts for Li-Oxygen Batteries, ACS Appl. Energy Mater. 2 (2019) 4144-4150. https://doi.org/10.1021/acsaem.9b00328.

[210] X. Li, C. Wen, M. Yuan, Z. Sun, Y. Wei, L. Ma, H. Li, G. Sun, Nickel oxide nanoparticles decorated highly conductive Ti_3C_2 MXene as cathode catalyst for rechargeable Li-O_2 battery, J. Alloys Compd. 824 (2020) 153803. https://doi.org/10.1016/j.jallcom.2020.153803.

[211] X. Li, C. Wen, H. Li, G. Sun, In situ decoration of nanosized metal oxide on highly conductive MXene nanosheets as efficient catalyst for Li-O_2 battery, J. Energy Chem. 47 (2020) 272-280. https://doi.org/10.1016/j.jechem.2020.02.016.

[212] P. Wang, D. Zhao, X. Hui, Z. Qian, P. Zhang, Y. Ren, Y. Lin, Z. Zhang, L. Yin, Bifunctional Catalytic Activity Guided by Rich Crystal Defects in Ti_3C_2 MXene Quantum Dot Clusters for Li-O_2 Batteries, Adv. Energy Mater. (2021) 2003069. https://doi.org/10.1002/aenm.202003069.

[213] D. Zhao, P. Wang, H. Di, P. Zhang, X. Hui, L. Yin, Single Semi-Metallic Selenium Atoms on Ti_3C_2 MXene Nanosheets as Excellent Cathode for Lithium-Oxygen Batteries, Adv. Funct. Mater. 31 (2021) 2010544. https://doi.org/10.1002/adfm.202010544.

[214] X. Han, N. Li, P. Xiong, M.G. Jung, Y. Kang, Q. Dou, Q. Liu, J.Y. Lee, H.S. Park, Electronically coupled layered double hydroxide/MXene quantum dot metallic hybrids for high- performance flexible zinc-air batteries, InfoMat (2021) 1-11. https://doi.org/10.1002/inf2.12226.

[215] Y. Chen, H. Yao, F. Kong, H. Tian, G. Meng, S. Wang, X. Mao, X. Cui, X. Hou, J. Shi, V_2C MXene synergistically coupling FeNi LDH nanosheets for boosting oxygen evolution reaction, Appl. Catal. B Environ. 297 (2021) 120474. https://doi.org/10.1016/j.apcatb.2021.120474.